R. & M. No. 2785
(12,430)
A.R.C. Technical Report

MINISTRY OF SUPPLY

AERONAUTICAL RESEARCH COUNCIL

REPORTS AND MEMORANDA

Notes on the Transonic Movement of Wing Aerodynamic Centre

By

S. B. GATES

LONDON: HER MAJESTY'S STATIONERY OFFICE

1956

NINE SHILLINGS NET

Notes on the Transonic Movement of Wing Aerodynamic Centre*

By

S. B. GATES

COMMUNICATED BY THE PRINCIPAL DIRECTOR OF SCIENTIFIC RESEARCH (AIR), MINISTRY OF SUPPLY

Reports and Memoranda No. 2785†

May, 1949

Summary.—These notes aim at providing a framework to display what is known of the backward movement of the aerodynamic centre of wing shapes likely to be used for transonic operation, as the flow progresses from incompressible through subsonic to supersonic, the shock-wave régime being ignored. A new geometrical parameter δ (*see* Figs. 1, 2) is taken as the main variable because (*a*) it gives a neat classification of the various wing shapes, (*b*) it expresses the results of supersonic theory in a simple form, (*c*) it simplifies the subsonic analysis by making direct use of the similarity law for three-dimensional compressible flow, and so (*d*) it is possible to display on one diagram most of the theoretical and experimental data at present available.

On the supersonic side, where very little experimental data is known in this country, the analysis is based on the conical solution by Puckett and Stewart[3, 4] for pointed tips; this has been extended on a simple but questionable assumption to cover blunt tips. On the subsonic side the laborious approximate theoretical methods have not yet yielded much data that is both systematic and reliable, and though model data is accumulating it inevitably lacks cohesion except in the case of delta wings. The work of R. T. Jones[8] on the aerodynamic centre of shapes so slender that it is independent of Mach number is linked up, so far as it goes, with the supersonic data, and should be extended.

When the existing fragments of the subject are assembled within this framework as in Table 1 and Fig. 13, the problem begins to get into focus and certain general trends are broadly discernible, but no very definite conclusions can be drawn except for pointed tips in general and delta wings in particular. These summaries do however show what will be the most profitable lines of research to illuminate quickly the whole subject, and recommendations are made to this end (*see* conclusions, section 9).

1. *Introduction.*—In passing from subsonic to supersonic flow the most important wing phenomenon after the drag rise is the rearward movement of the aerodynamic centre. At some stage in the transonic passage there will usually be a mixed flow at the surface where shock waves separate regions of supersonic and subsonic flow. This hard core of the transonic problem is mentioned here only to pass it by. Leaving it out, there is now an accumulation of linearised potential theory and experimental data covering the shockless subsonic and supersonic régimes. But the wing shapes that are being considered for several types of operation are extremely varied, the model data are not at all systematic, and the relevant supersonic theory is still not generally well known. Consequently the problem of the aerodynamic centre needs to be assembled from the existing fragments. These notes aim at supplying a framework which will display in an

* *Footnote*, 1952. This survey was made in 1948. Apart from a few footnotes to indicate roughly the advances since made in the subject, no attempt has been made to bring the paper up to date.

† R.A.E. Report Aero. 2325, received 25th June, 1949.

orderly fashion what is known of the subject. They refer exclusively to shapes which are likely to come into common use, *viz.*, those of which the half-plan is a trapezium or in the limit a triangle (Fig. 1).

2. *The Scope of Theory and Experimental Checks.*—The linearised potential theory is available for this problem in three sections :

(*a*) *Incompressible flow.*—As is well known, the solution can only be obtained by a laborious approximation in which the flat surface at incidence, and the wake behind it, are replaced by a continuous or discontinuous distribution of vorticity. There is in fact a continuing debate about the quickest and the mathematically soundest way out of this impasse. The labour involved in these lifting-surface theories has hitherto precluded any serious attempt to map systematic solutions over the variety of shapes involved. It is essential that this should ultimately be done, and a method recently devised by Schlichting[1] promises when fully developed to provide a relatively rapid and reliable tool for this job*.

(*b*) *Compressible subsonic flow.*—The Göthert development of the Prandtl-Glauert law[2] yields a simple rule for deriving the aerodynamic centres of any number of shapes at various Mach numbers, once the incompressible solutions are known. The incompressible aerodynamic centre of a given plan-form applies at Mach number M, to a plan form obtained by multiplying the lateral dimensions of the original shape by the factor $(1 - M^2)^{-1/2}$. The limits of application of this rule still need to be established experimentally, but it is clearly very useful as a rough guide in mapping the compressible field before the onset of shock waves.

(*c*) *Supersonic flow.*—Puckett and Stewart, in two important papers[3,4] have given the pressure distribution for conical flow over a delta wing of infinite extension. At about the same time Robinson[11] obtained the same results by a different method. Puckett and Stewart show how to derive from this the aerodynamic centres of all the shapes of Fig. 1 with *pointed tips*†, provided that the Mach angle is such that the flow over the finite wing remains conical.

In the trapezoidal wing, the Mach cone springing from the tip leading edge makes the flow non-conical and considerably complicates the theory. I have not yet had an opportunity of examining the American work in progress on this by Cohen, Langerstrom and others. A crude approximation, based on the pointed tip solution in what is likely to be the most practical case, is suggested below to cover smallish taper ratios.

In this summary of what is known in theory, it will be noticed that the vital shock-wave gap occurs between (*b*) and (*c*).

Puckett's and Stewart's work can be used to provide a very compact framework for a supersonic survey (Fig. 6). But as mentioned above there is no correspondingly explicit subsonic solution, and as yet very little in the way of systematic approximate solutions. Hence in using this diagram for the subsonic theory, all that can be done is to put in a few guiding lines and suggest what should be the general trend of the curves if we knew them.

When we come to fill in such a diagram with test data (Fig. 13), the situation is exactly reversed. There is a rather scattered collection of subsonic results which tend to cluster about those shapes, for instance the delta, the straight wing, and a few arrow-heads, on which model work has most concentrated. On the other hand, experimental support for the supersonic theory has hardly begun to appear. The only model check on pointed wings known to me gives excellent agreement.

* *Footnote,* 1952. Schlichting's method has run into unexpected mathematical difficulties, but in the interval Multhopp[2] has approached the matter differently and his method is now coming into use. Garner[13] has recently given some critical discussion of the methods now being used.

† Their calculation covers shapes (1) to (3) of Fig. 1, but it seems extensible in principle all the way to the reversed arrow-head.

3. *The Choice of Parameters.*—The aim of these notes being in effect to produce data sheets, the first step is to choose parameters which give the most compact and physically significant display.

The shape of a trapezium is defined by three non-dimensional quantities. These might be, for instance, the angles ω_0 and ω_1 of the leading and trailing edges and λ the taper ratio (Fig. 2). The three in commonest use in aerodynamic work are:

ϕ_n angle of sweep of the locus of points dividing the local chord in the ratio $n : 1 - n$. In what follows, such a point will be called the *n-chord point*; the quarter-chord point ($n = \frac{1}{4}$) is a familiar appellation

A aspect ratio

λ taper ratio.

In the following analysis we use a new variable δ defined as follows, *see* Fig. 2. The leading and trailing edges AP, BQ of the trapezium are produced to meet at C. Then δ is the ratio of BD, the projection of BC on the central line, to AB the root chord. δ is positive or negative according as C is downstream or upstream of B. The whole $\pm\infty$ range of δ separates the shapes in reference to flight into six classes—the arrow-head, the delta, the two lozenges, the reversed delta, and the reversed arrow-head*—as shown in Fig. 1.

Puckett and Stewart use the less convenient parameter a, which is the ratio of the projections of BC, AC on the central line. It easily follows that

$$a = \frac{\delta}{1 + \delta} = \frac{\tan \omega_0}{\tan \omega_1} . \qquad .. \quad .. \quad .. \quad .. \quad .. \qquad (1)$$

The proofs of this and other formulae are given in Appendix I.

For the second parameter we retain the taper ratio λ, and for the third we can use either aspect ratio A or sweep angle ϕ_n. The variables under discussion are connected by the formula:

$$A \tan \phi_n = 4 \frac{1 - \lambda}{1 + \lambda} (1 - n + \delta) . \qquad .. \quad .. \quad .. \quad .. \qquad (2)$$

Hence if we fix δ and λ we get a family of shapes—as sketched for example in Fig. 3—for which the variation of A with $\tan \phi_n$ is hyperbolic, large sweepback occurring with small aspect ratio and *vice versa.*

The family for which $\delta = n - 1$ is distinguished by the fact that its sweepback is zero, independent of A. Thus for example if $n = \frac{1}{4}$ we have at $\delta = -\frac{3}{4}$ a family with no sweep of the quarter-chord line, the familiar ' straight wing ' series.

It may help to grasp the connection between δ and sweepback to notice from (2) that for family of shapes for which aspect ratio and taper ratio are fixed, δ and $\tan \phi_n$ increase together in a linear relation.

The choice of what may seem at first the rather outlandish quantity δ as the main variable is made for two reasons:

(*a*) The supersonic solution for pointed tips, in what is probably the most important operational case, namely when the Mach cone lies outside the surface, shows that the aerodynamic centre depends only on δ; and the variation is moreover approximately linear.

(*b*) If, as in Fig. 3, one considers a family of shapes at constant δ and λ, it is clear that one member of the family can be derived from any other member by multiplying its lateral dimensions by a constant factor. The compressible law of similarity (section 2 (*b*))

* In this nomenclature only the delta is fully descriptive. Arrow-head and lozenge are used because they are roughly descriptive of the δ classes to which they refer when the aspect ratio is small, it being necessary to have some such shorthand in the course of the analysis.

can therefore be directly applied to such a family. It will appear in fact that in the Prandtl-Glauert régime the speed factor can be combined with the variables already discussed, and it follows that the aerodynamic centre is a function of δ, λ and βA or $\tan \phi_n/\beta$, where $\beta = \sqrt{(1 - M^2)}$.

The limitations of the framework of analysis indicated in equation (2) or Fig. 3 should be pointed out. It rests on the pointed-tip shape as prototype, and we may therefore expect that it would fail in practical application to shapes with very blunt tips. It is clear by considering equation (2) or the implications of Fig. 3 how the constant-chord swept wing slips through this net of classification. If $\lambda = 1$ and δ is finite, then either A or ϕ_n must be zero. Alternatively if $\lambda = 1$ and both A and ϕ_n are finite (the general case of the constant-chord wing), then δ must tend to ∞. Wings of finite aspect ratio and sweepback which approximate to constant chord therefore retreat towards infinity on a δ diagram. A separate analysis for the constant chord wing is used in section 8.3 below.

4. *Aerodynamic Centre on Simple Loading Assumptions.*—The main scheme is then to plot aerodynamic centre position as a function of δ, using additional parameters where necessary. It will be useful, as part of the framework of such a diagram, to indicate where the aerodynamic centre would be in simple cases of lift distribution.

At the spanwise section $\eta = y/s$ let the local aerodynamic centre be at the n-chord point and let the spanwise loading* be $f(\eta)$. The aerodynamic centre can then be found if n and f are known as functions of η. Let us first suppose that n is constant.

With this assumption it is shown in Appendix I that the distance of the aerodynamic centre behind the apex of the surface, in terms of the mean chord, is given by

$$h = \frac{2}{1+\lambda}\left\{n + (1-\lambda)(1-n+\delta)\frac{\int_0^1 \eta f(\eta)\, d\eta}{\int_0^1 f(\eta)\, d\eta}\right\} . \quad .. \quad .. \quad (3)$$

It is to be noted that this is a linear function of δ.

Two simple assumptions as to spanwise loading will be particularly useful.

(*a*) If the spanwise loading is proportional to the chord, so that $f(\eta) = 1 - \eta(1 - \lambda)$, we have from (3) for the position of the ' mean geometric n-chord point '

$$h_{\text{geometric}} = \frac{2}{1+\lambda}\left\{n + \frac{(1-\lambda)(1+2\lambda)}{3(1+\lambda)}(1-n+\delta)\right\} . \quad .. \quad .. \quad (4)$$

(*b*) If the spanwise loading is elliptic, so that $f(\eta) = \sqrt{(1-\eta^2)}$, we have for the position of the ' mean elliptic n-chord point '

$$h_{\text{elliptic}} = \frac{2}{1+\lambda}\left\{n + \frac{4}{3\pi}(1-\lambda)(1-n+\delta)\right\} . \quad .. \quad .. \quad .. \quad (5)$$

A good deal of use will be made of the reference points defined by (4) and (5) in what follows. For the present it may be noted that

(i) The mean geometric quarter-chord point ($n = \frac{1}{4}$) is the familiar ' quarter-chord point ' which is commonly used as a datum for aerodynamic centre in subsonic flow, and the corresponding elliptic point is equally useful as a reference.

(ii) It might be expected that the geometric and elliptic half-chord points would have an analogous use in sorting out supersonic results ; some refinements of this idea will be put to practical use below. The geometric half-chord point is of course the centre of area.

* The spanwise loading is defined as the ratio of the load per unit span at section η to the load per unit span at $\eta = 0$.

5. *Supersonic Conical Solution for Pointed Tips.*—5.1. *Delta Lift Distribution.*—This section is based entirely on Puckett's and Stewart's analysis[3, 4]. There are two régimes for conical flow over a delta wing. In the first the Mach cone is outside the wing surface; in the second the Mach cone intersects it. These will be called respectively the external and the internal solution. If ω_0 is the semi-vertical angle of the delta, and μ is the Mach angle, the speed parameter is

$$k = \tan \omega_0 \tan \mu$$

and so for the external solution we have $k < 1$ and for the internal solution $k > 1$.

In conical flow the lift distribution depends only on the angular co-ordinate ω measured from the apex of the delta.

The *external solution* is

$$\frac{\Delta p}{\alpha q} = \frac{4 \tan^2 \omega_0}{E[\sqrt{(1 - k^2)}]\sqrt{(\tan^2 \omega_0 - \tan^2 \omega)}} \quad \ldots \quad (6)$$

The *internal solution* is

$$\frac{\Delta p}{\alpha q} = \frac{4 \tan \omega_0}{\sqrt{(k^2 - 1)}} \cdot R\left[1 - \frac{2}{\pi} \sin^{-1}\sqrt{\left(\frac{\tan^2 \mu - \tan^2 \omega}{\tan^2 \omega_0 - \tan^2 \omega}\right)}\right] \quad \ldots \quad (7)$$

where Δp pressure below wing minus pressure above wing

α incidence

q dynamic pressure

E the complete elliptic integral of the second kind

and R signifies the real part of the function.

When $k \longrightarrow 1$ the internal and external solutions coincide:

$$\frac{\Delta p}{\alpha q} = \frac{8}{\pi} \frac{\tan^2 \omega_0}{\sqrt{(\tan^2 \omega_0 - \tan^2 \omega)}} \quad \ldots \quad (8)$$

5.2. *Speed Limits for Conical Solutions over Finite Wings.*—These solutions can be applied to all the finite shapes of Fig. 1 so long as the presence of the trailing edge does not affect the flow over the wing. Geometrically this means that the Mach cones springing from the tip and the rear end of the root chord must not cut the wing. This imposes speed limits for which each solution is valid for any given shape. These may be summarised, in terms of Mach angle μ, in the following table, which refers to Fig. 4 :—

Arrow-head $\omega_1 < \pi/2$	$\mu > \omega_1$	$\omega_1 > \mu > \omega_0$	$\omega_0 > \mu > 0$
	rear cone cuts wing	external solution	internal solution
Lozenge 1 $\omega_1 > \pi/2$	$\mu > \pi - \omega_1$	$\pi - \omega_1 > \mu > \omega_0$	$\omega_0 > \mu > 0$
	tip cone cuts wing	external solution	internal solution
$\pi - \omega_1 > \omega_0$			
Lozenge 2 $\omega_1 > \pi/2$	$\mu > \pi - \omega_1$		$\pi - \omega_1 > \mu > 0$
	tip cone cuts wing	no external solution	internal solution
$\pi - \omega_1 < \omega_0$			

It will be found that the limits for the external solution where it exists are given by

$$1 \leqslant k \leqslant |a| \quad \text{or} \quad \left|\frac{\delta}{1+\delta}\right| \quad .. \quad .. \quad .. \quad .. \quad .. \quad (9)$$

since the upper limit for μ is ω_1 or $\pi - \omega_1$, whichever is less than $\pi/2$.

It follows that if $M_{\min}$, $M_{\max}$ are the limits of Mach number for the external solution at a given δ, then

$$\sqrt{\left(\frac{M_{\min}-1}{M_{\max}-1}\right)} = \left|\frac{\delta}{1+\delta}\right|. \quad .. \quad .. \quad .. \quad .. \quad (10)$$

This relation is plotted in Fig. 5. The external solution ceases to exist when the shape becomes a rhombus, $\delta = -\frac{1}{2}$.

5.3. *Aerodynamic Centre.*—H, the distance of the aerodynamic centre behind the apex, divided by the mean chord, is obtained by integrating the pressures from (6) and (7) over the surface, the general formula being

$$H = \frac{\iint \Delta p r \cos\omega \,.\, r\, dr\, d\omega}{\bar{c}\iint \Delta p r\, dr\, d\omega}$$

where r, ω are polar co-ordinates from the apex and $\bar{c}$ is the mean chord.

The *internal solution* obtained by Puckett and Stewart from equation (7) is a function of a and k:

$$\tfrac{3}{2}H = \frac{\left(2 - \frac{a^2}{k^2} - \frac{a^4}{k^2}\right)\cos^{-1}\left(-\frac{a}{k}\right)}{(1-a^2)(1-a^2/k^2)^{3/2}} + \frac{a(3-a^2)\cos^{-1}\left(\frac{1}{k}\right)}{(1-a^2)(1-1/k^2)^{1/2}} + \frac{ak}{k^2-a^2} \quad .. \quad (11)$$
$$\frac{\cos^{-1}\left(-\frac{a}{k}\right)}{(1-a^2/k^2)^{1/2}} + \frac{a\cos^{-1}\left(\frac{1}{k}\right)}{(1-1/k^2)^{1/2}}$$

This is valid for $k \geqslant 1$.

For the *external solution* we note from (6) that as the speed term occurs as a factor of Δp, the aerodynamic centre must be independent of k and a function of a only. But the external and internal solutions coincide at $k = 1$. Hence the external solution is obtained from (11) by letting $k \to 1$. This gives for the *external solution*:

$$\tfrac{3}{2}H = \frac{a(4-a^2) + (2+a^2)\dfrac{\cos^{-1}(-a)}{\sqrt{(1-a^2)}}}{(1-a^2)\left[a + \dfrac{\cos^{-1}(-a)}{\sqrt{(1-a^2)}}\right]} \quad .. \quad .. \quad .. \quad .. \quad .. \quad (12)$$

for which the range of validity is

$$1 \leqslant k \leqslant |a|.$$

5.4. *Numerical Results for Aerodynamic Centre.*—The computation of Ref. 3 covers the range $\pm 0{\cdot}8$ in a, or 4 to $-0{\cdot}45$ in δ; that is, from the narrow arrow-head almost to the rhombus. The external and internal solutions are plotted together on a δ base with k as parameter in Fig. 6. The single curve for the external solution is taken from Table 1 of Ref. 3 and is fairly accurate; the family of curves for the internal solution are taken from a small diagram (Fig. 16 of Ref. 3) and are much less accurate.

The following points should be noted:

(*a*) The external curve has small curvature. This will be elaborated below.

(*b*) For arrow-heads the aerodynamic centre is furthest back for external flow and moves forward as the speed increases through the internal flow régime. The situation is reversed for lozenges.

(*c*) For arrow-heads the forward movement of aerodynamic centre is greatest when the Mach cone enters the surface. It slows down as speed increases, and the variation has apparently ceased when $k = 2{\cdot}5$.

(*d*) The curves all intersect at $\delta = 0$. This emphasises the central position of the delta in the development of the theory. The aerodynamic centre of a delta wing is at its centre of area for all supersonic speeds.

In order to relate this diagram more clearly to the shapes involved and the actual position of the aerodynamic centre in plan, sketches have been added of typical shapes at $\delta = 4$, 2, $0{\cdot}5$ (arrow-head); $\delta = 0$ (delta); and $\delta = -0{\cdot}25$ (lozenge). At each value of δ, two sketches are shown, giving the flow conditions for the external and internal régimes. On these are marked P the (constant) aerodynamic centre for external flow, and P_2 the aerodynamic centre at $k = 2$ for internal flow. The difference between P and P_2 at any δ gives a clear idea of the total shift in aerodynamic centre at supersonic speeds in relation to the general shape of the wing.

It will be realised of course that the shape sketched at any value of δ is only one of a family of shapes thereby defined (*see* Fig. 3).

5.5. *Approximations to the External Solution.*—Current opinion seems to be settling in favour of designing a supersonic wing with so much sweepback that it operates with conical flow inside the Mach cone. The argument that this minimises the wave drag while retaining a high value of the lift slope probably outweighs the penalty noted above that the aerodynamic centre is in general furthest back in this régime. We may therefore concentrate on the simple external solution.

In Fig. 7 the external solution is plotted with the straight lines (obtained from equations (4), (5)), representing the mean geometric half-chord point and the mean elliptic half-chord point. The geometric half-chord line intersects the exact solution at $\delta = 0$, as it must do since the delta's aerodynamic centre is its centre of area; but for arrow-heads the aerodynamic centre is always to the rear of the geometric half-chord point. On the other hand the elliptic half-chord line is a rough first approximation to the internal solution: its slope $8/3\pi$ is in fact the slope of the external solution at $\delta = 0$.

We can get a closer linear approximation to the external solution by assuming an elliptic spanwise lift distribution and choosing the best value n of the chordwise loading point. The straight line AB, with $n = 0{\cdot}45$, is a fair approximation between $\delta = -0{\cdot}5$ and $1{\cdot}5$. The straight line CD, with $n = 0{\cdot}61$, is a rougher approximation between $\delta = 1{\cdot}5$ and 4. This means that wings between $\delta = -0{\cdot}5$ and $1{\cdot}5$ behave on the whole as if they were elliptically loaded at the $0{\cdot}45$-chord point, and between $\delta = 1{\cdot}5$ and 4 as if they were elliptically loaded at the $0{\cdot}61$-chord point.

To give a preliminary idea of the position of the subsonic aerodynamic centre for pointed tips, plots of the mean geometric and elliptic quarter-chord points are shown on this diagram.

5.6. *Spanwise and Chordwise Lift Distribution for the External Solution.*—Equation (6) gives the lift distribution on lines radiating from the apex, but for practical purposes the spanwise and chordwise distributions are required; this moreover will throw some further light on the analysis of section 5.5. Using equation (6) we can express the spanwise loading f and the local aerodynamic centre n_l (*see* section 4) as functions of the dimensionless spanwise co-ordinate η. Details of these integrations are given in the Appendix II. The results are:

$$f = \sqrt{[(1-\eta^2) + 2\delta(\eta-\eta^2)]}\,, \quad \ldots \quad \ldots \quad \ldots \quad \ldots \quad \ldots \quad \ldots \quad (13)$$

$$n_l = \tfrac{1}{2} + \frac{(1+\delta)^2\eta^2}{2(1-\eta)\sqrt{[1+2\delta\eta-(1+2\delta)\eta^2]}} \cdot \log\left\{\frac{1+\delta\eta+\sqrt{[1+2\delta\eta-(1+2\delta)\eta^2]}}{(1+\delta)\eta}\right\} - \frac{(1+\delta)\eta}{2(1-\eta)}\,. \quad (14)$$

These formulae, which are plotted in Figs. 8 and 9, show that

(*a*) The delta is elliptically loaded but its local aerodynamic centre is on the whole further forward than half-chord.

(*b*) As δ increases from zero the spanwise loading becomes super-elliptic (very markedly so for the narrow arrow-heads); while the local aerodynamic centre moves on the whole strongly forward. These contrary tendencies produce a mean aerodynamic centre, over the whole range of δ, which is not far removed from the mean elliptic half-chord point (Fig. 7). For a fuller discussion *see* Appendix II.

5.7. *Experimental Check on Supersonic Theory.*—Unfortunately no supersonic model tests on pointed arrow-heads seem to have been published. The only relevant data known to me is in Ref. 5 where Squire summarises some Göttingen tests on the lozenge $\omega_0 = 33$ deg, $\delta = -\frac{1}{4}$, $a = -\frac{1}{3}$ at $M = 1{\cdot}20, 1{\cdot}45, 1{\cdot}99$. This is case B of the report; case A gives non-conical flow. Theoretical and experimental values of aerodynamic centre H and lift slope $dC_l/d\alpha$ are given below:

Lozenge $\omega_0 = 33$ deg, $\delta = -\frac{1}{4}$, $a = -\frac{1}{3}$.

M	k	Type of solution	H		$dC_L/d\alpha$	
			theory	experiment	theory	experiment
1·20	0·44	external	1·12	1·10	3·31	3·05
1·45	0·70	external	1·12	1·10	2·89	2·81
1·99	1·15	internal	slightly less than 1·12	1·10	2·20	2·11

This shows very good agreement on aerodynamic centre and 5 per cent to 10 per cent discrepancy on lift slope.

6. *Supersonic Aerodynamic Centre for Blunt Tips.*—When pointed tips are cut off parallel to the centre-line the theory becomes much more difficult because it must take account of the Mach cone springing from the tip leading edge, which now cuts the wing. Work has apparently been done on these tip corrections by Cohen, Langerstrom and others in America, but their theories have not yet reached me. We may perhaps make a very rough shot at a general trend by assuming that the linear approximation of section 5.5 to the external solution for pointed tips ($\lambda = 0$), applies also to finite values of λ. This amounts to suggesting that when pointed tips are cut off, the aerodynamic centre remains approximately at the elliptic 0·45-point in the range $-\frac{1}{2} < \delta < 1{\cdot}5$, and in the neighbourhood of the elliptic 0·61-point in the range $1{\cdot}5 < \delta < 4$. Putting $n = 0{\cdot}45$ and $0{\cdot}61$ in equation (5), this gives :—

$$\left.\begin{aligned} H &= \frac{1{\cdot}37 - 0{\cdot}47\lambda}{1+\lambda} + 0{\cdot}85\,\frac{1-\lambda}{1+\lambda}\,\delta, \quad -\tfrac{1}{2} < \delta < 1{\cdot}5 \\ &= \frac{1{\cdot}55 - 0{\cdot}33\lambda}{1+\lambda} + 0{\cdot}85\,\frac{1-\lambda}{1+\lambda}\,\delta, \quad 1{\cdot}5 < \delta < 4 \end{aligned}\right\} \quad \ldots \quad (15)$$

The speed limits would be the same as for pointed tips.

The straight lines (15) are plotted in Fig. 10 up to $\lambda = \frac{3}{4}$.

7. *Subsonic Shockless Compressible Flow (Theory).*—7.1. *Göthert's Similarity Law.*—Göthert's three-dimensional extension of the Prandtl-Glauert law (*see* for instance Ref. 6) shows that the

non-compressible aerodynamic centre for any wing applies also to flow at Mach number M if the lateral dimensions are multiplied by $1/\beta$, where $\beta = \sqrt{(1 - M^2)}$. Thus if A, A_0 are the aspect ratios of the compressible and incompressible wing we have

$$\left.\begin{aligned} A &= \frac{A_0}{\beta}, \\ \text{and similarly, as regards sweepback} & \\ \tan\phi &= \beta \tan\phi_0 \end{aligned}\right\} \quad \ldots \quad (16)$$

Now it has already been pointed out (*see* Fig. 3) that if λ and δ are constant, the family of shapes are derived by this law of lateral dimensions. It follows from (16) that at given δ and λ the aerodynamic centre is a function of βA only, or alternatively of $\tan\phi/\beta$. Thus within the limits of this theory, we can suppress the speed an an independent variable and say that the aerodynamic centre is a function only of δ, λ and βA (or $\tan\phi/\beta$).

Hence if λ is fixed we can theoretically show the whole variation of aerodynamic centre in this régime by plotting curves of constant βA on the H, δ diagram, and these curves can be constructed entirely from incompressible solutions. There is here a wide field for theoretical work which urgently needs working on. To show the lack of systematic work of this nature, there is nothing to put on the pointed-tip diagram of Fig. 7 except some calculations by De Young[7] using Weissinger's method, which itself is suspect because it ignores the downwash singularity at the centre of a kinked vortex line. The result shown is a mean of curves for $\beta A = 2{\cdot}5$ and $4{\cdot}5$, which are almost indistinguishable on the H scale used. It should be noted that the calculated curve, for what it is worth, lies between the elliptic and geometric quarter-chord lines.

7.2. *Variation with Aspect Ratio.*—Although the subsonic region of the aerodynamic-centre diagram plotted on a δ base cannot yet be filled in from theory, we can get some idea of the trend of the variations with A at constant δ, λ by considering the limits of large and small aspect ratio.

(*a*) *Large aspect ratio.*—Consider the shape reached in a δ, λ family such as that of Fig. 3 when the span is extended towards infinity. It is important to notice that in proceeding to $A \to \infty$ in this way we are working at constant taper ratio λ, and not as is more usual at constant chord. When the span gets very large it can be divided spanwise into a series of elements, of large span, each of which is effectively a piece of a two-dimensional wing, of small sweepback, whose chord is the mean chord of the large spanwise section considered. The local aerodynamic centre of this large element must therefore be at the quarter-chord point, and summing for all such elements it follows that the aerodynamic centre of the whole wing tends to the mean geometric quarter-chord point as $A \to \infty$.

The geometrical quarter-chord line for given λ is therefore very useful on the δ-diagram in giving at each point the limiting position of the aerodynamic centre of the δ, λ family as $A \to \infty$. The formula is

$$H_{A \to \infty} = \frac{1}{2(1+\lambda)} \left\{ 1 + \frac{(1-\lambda)(1+2\lambda)}{(1+\lambda)} \left(1 + \tfrac{4}{3}\delta\right) \right\}. \quad \ldots \quad (17)$$

(*b*) *Small aspect ratio.*—R. T. Jones' theory of the slender pointed aerofoil[8] gives at once the position of the aerodynamic centre for all the shapes we are considering, except the arrow-heads, as $A \to 0$.

His solution for the pressure distribution of a slender delta (*see* Fig. 11a) may be written

$$\frac{\Delta p}{\alpha q} = \frac{4 \tan^2 \omega_0}{\sqrt{(\tan^2 \omega_0 - \tan^2 \omega)}}, \quad \ldots \quad (18)$$

ω_0 being small.

This agrees with the external supersonic solution (6) if ω_0 is small and μ is finite, for then $k \to 0$ and $E[\sqrt{(1-k^2)}] \to 1$.

The speed range for which (18) is valid is indicated by Jones' general argument. He shows that if ϕ is the velocity potential of a slender delta moving in the x-direction, then $\partial^2\phi/\partial x^2$ is small compared with $\partial^2\phi/\partial y^2$ and $\partial^2\phi/\partial z^2$. Thus, considering the general linearised equation

$$(1 - M^2)\frac{\partial^2\phi}{\partial x^2} + \frac{\partial^2\phi}{\partial y^2} + \frac{\partial^2\phi}{\partial z^2} = 0\,,$$

Jones' theory amounts to neglecting $(1 - M^2)\partial^2\phi/\partial x^2$ in comparison with the other terms, and hence is valid for all speeds until M becomes so large that the term above ceases to be negligible.

Jones thus shows that the aerodynamic centre of a slender delta is at its centre of area for all speeds, subsonic and supersonic, and thus confirms the supersonic theory in the limit $A \to 0$.

We may sum up by saying of deltas that if the aspect ratio is large the aerodynamic centre starts in the neighbourhood of half the root chord at slow speeds, moves back in the subsonic region until shock waves occur, and settles down at the centre of area at supersonic speeds. But if the aspect ratio is small enough the aerodynamic centre starts at the centre of area and remains there: the slender delta goes through unchanged.

Jones extends his theory from the delta to the pointed lozenge (Fig. 11b) and the blunted lozenge (Fig. 11c) by arguing that the surface to the rear of the forward triangle contributes no lift. His reasoning is not perhaps completely convincing, but if it is accepted the aerodynamic centre of Figs. 11a, 11b and 11c remains at P. It is simple geometry to show from this that H for the blunted lozenge δ, λ, A tends to the limit

$$H_{A \to 0} = \frac{4}{3}\frac{1-\lambda}{1+\lambda}(1+\delta) \quad .. \quad .. \quad .. \quad .. \quad .. \quad .. \quad .. \quad (19)$$

as $A \to 0$. This is valid for $-1 < \delta \leqslant 0$.

For the pointed lozenge ($\lambda = 0$) we have simply

$$H_{A \to 0} = \tfrac{4}{3}(1+\delta)\,. \quad .. \quad .. \quad .. \quad .. \quad .. \quad .. \quad .. \quad (20)$$

This straight line for the pointed lozenge, which of course cuts the external supersonic solution at $\delta = 0$, is plotted in Fig. 7. So far as it goes, it gives the aerodynamic centre of pointed lozenges which are so slender that they go through the speed of sound without aerodynamic-centre movement. It is not difficult to show why this ' no-change ' line differs, except at $\delta = 0$, from the external supersonic solution. This arises because of the speed range carried by each point of the external supersonic solution. As already pointed out, the Mach angle for an arrow-head must lie between ω_0 and ω_1, and there is a similar condition for lozenges. Thus for all these shapes M must tend to ∞ as $A \to 0$. The delta is the only shape for which the speed range of the external supersonic solution remains finite as $A \to 0$.

(*c*) *Comparison of the two limits.*—In Fig. 12, $H_{A \to 0}$ and $H_{A \to \infty}$ are plotted together from equations (17), (19) in the negative δ range for which they are both known, with $\lambda = 0, \frac{1}{4}, \frac{1}{2}, \frac{3}{4}$.

This diagram shows that the direction of the total movement of aerodynamic centre as A goes from ∞ to 0 depends on the taper ratio. In the case of deltas, for example, it is rearward for pointed tips, zero at a value of λ slightly exceeding $\frac{1}{4}$, and forward for more blunted tips. For straight wings the change is always forward.

It is unfortunate that this diagram cannot be extended to the arrowheads ($\delta > 0$) because Jones' theory does not at present cover the slender arrow-head (Fig. 11d). The calculation is a

difficult one, but is of such intrinsic interest that it is being attempted*. It can be predicted however that the no-change line for pointed arrow-heads—the unknown continuation of PQ of Fig. 7 at positive δ—will lie wholly above the external solution, since it can only cut the latter at Q.

8. *Subsonic Experimental Data.*—The model results available for examination within the framework developed here are drawn from the British, American and German sources of Refs. E1 to E17. They are tabulated in Tables 1 and 2 and plotted in Figs. 13 and 14. Table 1 and Fig. 13 for tapered wings cover a range of δ from $-\frac{3}{4}$ (zero quarter-chord sweepback) to about 2, corresponding to fairly narrow arrow-heads. Table 2 and Fig. 14 display the special case of untapered wings which do not conveniently fit in to the general framework ($\delta \to \infty$).

8.1. *Tapered Wings, Table* 1.—The tests comprise sporadic studies, from various angles and with various objects, of novel plan-forms as they were suggested by the developing problem of high-speed flight. Thus no general systematisation can be expected. The work was done mainly at low speed and smallish Reynolds number; the aerodynamic centre is derived from the pitching-moment slope between $C_L = 0$ and $0{\cdot}2$. When high-speed tests are used, the results quoted are for values of M well below any sharp change in drag or pitching moment slope. Table 1 gives the experimental parameters in the form suggested by this analysis, and ends by comparing the measured aerodynamic centre H_{subsonic} with three other points:

(*a*) The mean geometric quarter-chord point. This is the commonly used aerodynamic datum in subsonic analysis. It is usual to work with h_0 the distance of the aerodynamic centre behind the nose of the mean chord. h_0 is obtained by adding $0{\cdot}25$ to the difference between H_{subsonic} and the quarter-chord point.

(*b*) The mean elliptic quarter-chord point, which is another common landmark in subsonic surveys of this nature.

(*c*) The mean elliptic $0{\cdot}45$-point. This can be called the supersonic aerodynamic centre ($H_{\text{supersonic}}$) if the reservations discussed in section 6 are again emphasised. It is a good approximation to the external supersonic solution for pointed tips ($\lambda = 0$) if δ lies between $-\frac{1}{2}$ and $1\frac{1}{2}$. There is some experimental support for identifying it with the aerodynamic centre at $\lambda = \frac{1}{2}$, but its general application to blunt tips is only suggested as a rough guide.

The last column of the tables gives with these reservations the difference between the theoretical $H_{\text{supersonic}}$ as defined above and the measured H_{subsonic}. This transonic movement of the aerodynamic centre has been starred where, for $\lambda = 0$, it is firmly grounded; for other values of λ it is subject to the reservations of section 6.

8.2. *Tapered Wings, Fig.* 13.—The material of Table 1, which assembles the experimental values of $H_{\text{subsonic}} = F(\delta, \lambda, \beta A)$ should properly be analysed by isolating each variable in turn. For example it is important to know the nature of the variation of H_{subsonic} with βA at constant δ, λ. The bag is so mixed however, that it seems best in this preliminary survey to plot all the results on one δ diagram, adding a framework which will help to elucidate the general trends of what can be deduced. This has been done in Fig. 13, where the values of βA and λ for each experimental point are tabulated.

8.2.1. *Framework of the diagram.*—As a frame of reference the straight-line plots of the three points discussed in section 8.1 are drawn for four values of λ:—0, $\frac{1}{4}$, $\frac{1}{2}$, $\frac{3}{4}$. Before studying the picture in detail these four triads of reference lines should be clearly distinguished and their significance noted.

Consider for instance the framework for $\lambda = 0$, where the interpretation is most firmly grounded. The uppermost chain-dotted line (elliptic $0{\cdot}45$ point) is seen to be a fair approximation to the external supersonic solution, $H_{\text{supersonic}}$. The lower full line (geometric quarter-point) is the limit of H_{subsonic} for large aspect ratio. Let us note what happens when a given wing, designed to

* *Footnote,* 1952. The solution has since been obtained by Mangler[14].

operate at an ' external ' supersonic speed, goes through to its operational speed. At low speed the aerodynamic centre will be somewhat aft of the geometric quarter-point and will move back until at some value of β, determined by the combination of sweepback and section characteristics, shock waves appear and the βA law breaks down. This régime will be followed*, when $M > 1$, by a supersonic non-conical régime of which the solution is not known to me ($\mu > \omega_1$). And finally, when $\mu < \omega_1$ we arrive at the external supersonic régime represented roughly, for a considerable range of speeds, by the elliptic 0·45-point.

It is possible of course that the aerodynamic centre may temporarily recede beyond the elliptic 0·45-point in the shock-wave régime or the following non-conical régime. Remembering this reservation, it may be said that for $\lambda = 0$ the boundaries of the reference triad define a transonic band which gives the maximum difference between the positions of the aerodynamic centre at operational speed and at landing. The transonic band diverges markedly with increasing δ, and so a penalty in the use of pronounced pointed arrow-heads is indicated.

If the same argument is used for blunt types ($\lambda = \frac{1}{4}, \frac{1}{2}$, etc.) it is noted that the two subsonic reference lines tend to coincide, and so the transonic band narrows qualitatively to the parallel one of depth 0·2 between the elliptic 0·45 and quarter-points. This would mean that for taper ratios greater than about $\frac{1}{4}$ we have at most a transonic band of about 0·2 to face, independent of δ. This conclusion would however be very rash without further confirmation than is given in section 6 that the supersonic aerodynamic centre remains in the neighbourhood of the elliptic 0·45-point for moderate values of taper ratio.

8.2.2. *Trends of the model results.*—A glance at the disposition of points on the diagram shows where experimental interest has concentrated. Deltas and blunted deltas ($\delta = 0$) are heavily represented; work on blunt arrow-heads gives points strung out mainly on the subsonic reference lines for $\lambda = \frac{1}{4}$ and $\frac{1}{2}$; and there is some scattered work on the straight wing (zero quarter-chord sweepback, $\delta = -\frac{3}{4}$).

(*a*) *Deltas and blunted deltas* (*points* 20 *to* 34).—Points 20 to 26, for $\lambda = 0$, are the only systematic group on the diagram, though they are not all from the same experiment. They show a fairly consistent backward movement as βA decreases from 4 to 1, and indicate the large reduction in transonic shift which follows the use of small aspect ratio.

Points 27 to 34, for blunted deltas, have λ varying from 0·12 to 0·50 and βA from 1·33 to 6·0. Subdivisions are points 27 to 29 with λ about 0·13, and points 30 to 32 with λ about 0·25. The λ, βA grouping is too scattered to sort out the variation.

(*b*) *Blunted arrow-heads* (*points* 35 *to* 52).—These cover a range of δ from about 0·3 to 2·4.

Points 35, 39, 42, 43, 47 are with one exception at $\lambda = 0{\cdot}25$; A varies from 3 to 5.

Points 36 to 38, 40, 44, 45, 48 to 52 are at $\lambda = 0{\cdot}5$ with βA varying from 2·25 to 6. There are three pairs of points (36, 37), (44, 45), (48, 49) for which βA varies at constant values of δ and λ.

Most of these results show the aerodynamic centre to be well behind the mean geometric quarter-chord point.

(*c*) ' *Straight* ' *wings* ($\phi_{1/4} = 0$. $\delta = -\frac{3}{4}$). *Points* 3 *to* 15.—In this scattered group, λ ranges from 0 to 0·625 and βA from 3 to 12.

Two subdivisions can be noticed:

(i) Points 4 to 8, at $\lambda = 0{\cdot}2$, with βA between 10 and 12.

(ii) Points 10 to 13, at $\lambda = 0{\cdot}5$, with βA between 3 and 6.

In neither sub-group are the values numerous or consistent enough to sort out the variation of H with βA.

* Except for deltas, where the external supersonic régime starts at $M = 1$.

8.2.3. *Blanks on the map.*—It is clear enough that blanks predominate on the map of Fig. 13, and that further exploration concentrated on establishing the variation of H_{subsonic} with βA at a few significant values of δ, λ will be of more value than any amount of sporadic work dotted about the diagram.

It is proposed that a minimum programme should aim at reinforcing the delta work, and should investigate arrow-heads at two values of δ, $\frac{3}{4}$ and $1\frac{1}{2}$. In each case two taper families should be explored, $\lambda = 0$ and $\frac{1}{2}$, over at least 3 values of βA, in the range 1 to 6.

These ranges summarise as:

δ 0, $\frac{3}{4}$, $1\frac{1}{2}$

λ 0, $\frac{1}{2}$

βA three values in range 1 to 6,

a total of 18 wings which should be studied both theoretically and experimentally at low speed ($\beta \simeq 1$). There are obvious advantages in having the experimental work done if possible in one tunnel, and the theoretical work by one method.

8.3. *Untapered Wings.*—In analysing the untapered wing results ($\lambda = 1$) we use, instead of δ, the ratio to the chord of the central projection of the semi-trailing-edge; this is called γ (*see* inset Fig. 14). This gives the simple relation:

$$A \tan \phi = 2\gamma . \quad .. \quad .. \quad .. \quad .. \quad .. \quad (21)$$

Thus H_{subsonic} may be regarded as a function of γ and βA or $\tan \phi/\beta$.

The results are shown in Table 2 and Fig. 14, which are analogous to Table 1 and Fig. 13 except as follows:

(*a*) All the experimental results are for low speed ($\beta \simeq 1$).

(*b*) No suggestion is made as to the supersonic aerodynamic centre, since any argument from pointed tips is certainly inapplicable here.

(*c*) Two series of calculations have been included:

(i) Wieghardt's analysis[9] of rectangular wings of small aspect ratio.

(ii) Falkner's calculations (E14) in the ranges $\gamma = 0$ to 3, $A = 1$ to 6.

8.3.1. *Discussion of Fig.* 14.—(*a*) The numerous results for rectangular wings ($\gamma = 0$) are not shown on the main diagram, but are plotted against A in the figure inset, where Wieghardt's theoretical curve is exhibited with the experimental results and Falkner's calculations. The tendency for the aerodynamic centre to move forward from the quarter-chord point towards the leading edge as the aspect ratio decreases is very well established, although its physical significance is obscure. These and allied questions will be more fully discussed in a forthcoming paper by Thomas[10].

(*b*) A first glance at the disposition of points on the main diagram would suggest a general trend to cross first the elliptic quarter-chord line and then the geometric quarter-chord line as γ increases. This however is of doubtful significance as it ignores the large variation (1 to 6) in aspect ratio. When the points are considered in more detail, there are few clues to the variation with aspect ratio at any value of γ other than zero. We conclude, as in the discussion of Fig. 13, that what is wanted is a cross-section of results from theory and experiment, over the range $A = 1$ to 6, for at least two values of γ, say 1 and 2.

9. *Conclusions.*—(*a*) The choice of δ as the main parameter in sorting out what is known of the transonic shockless shift of aerodynamic centre appears to justify itself on the following grounds :

(i) It gives a tidy classification of the various trapezoidal and triangular half plan-forms which are candidates for transonic operation.

(ii) On the supersonic side it simplifies the theoretical results for conical flow.

(iii) On the subsonic side it permits direct application of the compressible similarity law, and so eliminates the speed as an independent variable.

(iv) It leads to a display of the fragmentary data of the subject (*see* Fig. 13) which, while as yet very incomplete, gives a coherent view of what is known and in what direction research should proceed.

(*b*) The aim of these notes has been to establish a framework within which theoretical and experimental data can be clearly assessed. For various reasons the blanks on the map are at present such that broad practical conclusions must be tentative. The supersonic limit of aerodynamic centre is well established theoretically for pointed tips. American theoretical work on the effect of blunting the tips has not yet been examined, but a rough rule is suggested here. On the subsonic side there is very little systematic theoretical data, and the model results, though fairly numerous, lack fruitful correlation except in two corners of the field, the deltas and the rectangular wings.

(*c*) Tentative conclusions as to transonic movement are as follows :

(i) If a wing with *pointed tips* is designed to operate supersonically in the external conical régime, its supersonic aerodynamic centre is approximately at the elliptic 0·45-point; whereas its aerodynamic centre at slow speed will not be further forward than the geometric 0·25-point. The difference between these points therefore gives the upper limit of transonic movement, ignoring what happens between the appearance of shock waves and the establishment of the conical flow. On the δ-diagram this gives a transonic band which diverges as δ increases. Its depth is about 0·23 for straight wings, 0·36 for deltas, and 0·56 for the arrow-head family $\delta = 1$ (Fig. 13).

(ii) If it is assumed that the effect of *blunting the tips* is to leave the supersonic aerodynamic centre in the neighbourhood of the elliptic 0·45-point the transonic band, as defined above, becomes roughly of depth 0·2, independent of δ, for taper ratios exceeding 0·25. The optimistic conclusion that we can by blunting the tips confine the transonic movement to about 0·2 for any wing cannot however be accepted without further experimental support. Study of theoretical American work in progress will no doubt elucidate the matter.

(*d*) Emphasis must be laid on the need for filling up the picture in the following directions:

(i)* Systematic subsonic theoretical and model data to establish the variation of H with βA for a few typical values of δ and λ. A short programme which would throw much light on the whole matter would comprise the following ranges (*see* section 8.2.2) :—

$$\left.\begin{array}{ll} \delta & 0, \frac{3}{4}, 1\frac{1}{2} \\ \lambda & 0, \frac{1}{2} \\ \beta A & \text{3 values in range 1 to 6} \end{array}\right\}.$$

(ii)* Extension of R. T. Jones' theory to calculate H for slender arrowheads (δ positive, A small).

Acknowledgements.—I am much indebted to H. H. B. M. Thomas for helpful discussions in the course of this work, particularly as to the details of Appendix II; and to Mrs. Collingbourne and Miss Ward for assembling and displaying the experimental data.

* *Footnote,* 1952. Surveys similar to that suggested in (i) are now in progress. The solution of (ii) is now known.

LIST OF SYMBOLS

The notation is mainly defined in the diagrams, as follows:

Figs. 1 and 2. c_r, δ, a, n, λ, ω_0, ω_1, ϕ_n

Fig. 14. γ

Fig. 15. x, y, s, s'

Fig. 16. x_0, x_1, ω

In addition the following may be noted:—

H	Distance of aerodynamic centre behind the apex, divided by the mean chord $\bar{c}$
$\eta = y/s$	Non-dimensional lateral co-ordinate
$f(\eta)$	Spanwise loading; lift per unit span at η divided by lift per unit span at $\eta = 0$
n-chord point	Point dividing chord in ratio $n : 1 - n$
Mean geometric / elliptic n-chord point	Aerodynamic centre when the local aerodynamic centre is constant at n and the spanwise loading is geometric / elliptic
$h_{\text{geometric}}$ / h_{elliptic}	Distance of mean geometric / elliptic n-chord point behind apex, divided by mean chord
μ	Mach angle
$k = \dfrac{\tan \omega_0}{\tan \mu}$	
$u = x \tan \omega_0$	
ω	Angular co-ordinate from apex
$\beta = \sqrt{(1 - M^2)}$	
A	Aspect ratio
λ	Taper ratio $\left(\dfrac{\text{tip chord}}{\text{root chord}}\right)$

REFERENCES

No.	Author	Title, etc.
	General	
1	H. Schlichting and W. Kahlert ..	Calculation of lift distribution of swept wings. A.R.C. 12,238. October, 1948. (Unpublished.)
2	B. Göthert	Berechnung der Geschwindigkeitsfeldes von Pfeilflügeln bei hohen Unterschallgeschwindigkeiten. *Lilienthal Gesellschaft für Luftfahrtforschung*, Bericht 127. September, 1940.
3	A. E. Puckett and H. J. Stewart ..	Aerodynamic performance of delta wings at supersonic speeds. *J. Ae. Sci.*, Vol. 14, No. 10. October, 1947.
4	H. J. Stewart..	The lift of a delta wing at supersonic speeds. *Quarterly of Applied Mathematics*, Vol. IV, No. 3. October, 1946.
5	H. B. Squire	German wind-tunnel tests of a wing of small aspect ratio at subsonic and supersonic speeds. A.R.C. 9562. February, 1946. (Unpublished.)
6	R. Dickson	The relationship between the compressible flow round a swept-back aerofoil and the incompressible flow round equivalent aerofoils. A.R.C. 9986. August, 1946. (Unpublished.)
7	J. De Young	Theoretical additional span loading characteristics of wings with arbitary sweep, aspect ratio and taper ratio. N.A.C.A. Tech. Note 1491. December, 1947.
8	R. T. Jones	Properties of low aspect ratio pointed wings at speeds below and above the speed of sound. A.R.C. 9483. March, 1946.
9	K. Wieghardt	Chordwise load distribution of a simple rectangular wing. N.A.C.A. Tech. Memo. 963. December, 1948.
10	H. H. B. M. Thomas	Similarity laws for wings in three-dimensional compressible flow. A.R.C. 13,154. December, 1949. (Unpublished.)
11	A. Robinson	Aerofoil theory of a flat delta wing at supersonic speeds. R. & M. 2548. September, 1946.
	Additional References (1952)	
12	H. Multhopp	Methods for calculating the lift distribution of wings (subsonic lifting-surface theory). R. & M. 2884. January, 1950.
13	H. C. Garner	Swept-wing loading. A critical comparison of four subsonic vortex-sheet theories. C.P. 102. July, 1951.
14	K. W. Mangler	Calculation of the pressure distribution over a wing at sonic speeds. R. & M. 2888. September, 1951.
	Experimental (*E*)	
E1	W. A. Mair, S. P. Hutton and H. E. Gamble.	High-speed tunnel tests on the *Mosquito*. A.R.C. 8525. December, 1944. (Unpublished.)
E2	R. F. Anderson	The experimental and calculated characteristics of 22 tapered wings. N.A.C.A. Report 627. 1938.
E3	G. Hieser and C. F. Whitcomb ..	Investigation of the effects of a nacelle on the aerodynamic characteristics of a swept wing and the effects of sweep on a wing alone. N.A.C.A. Tech. Note 1709. October, 1948.
E4	A. B. Haines and W. Port.. ..	High-speed tunnel tests on a series of 14 per cent thick wings of varying sweepback and taper ratio. A.R.C. 12,179. October, 1948. (Unpublished.)
E5	J. A. Shortal and B. Maggin ..	Effect of sweepback and aspect ratio on longitudinal stability characteristics of wings at low speeds. N.A.C.A. Tech. Note 1093. July, 1946.
E6	P. E. Purser and M. L. Spearman	Wind-tunnel tests at low speed of swept and yawed wings having various plan-forms. N.A.C.A. Research Memo. L7D23. May, 1947.

REFERENCES—*continued*

No.	*Author*	*Title, etc.*
	Experimental (E)—continued	
E7	J. S. Thompson and W. Port ..	High-speed wind-tunnel tests on a jet-propelled flying boat (E6/44). A.R.C. 8995. September, 1945. (Unpublished.)
E8	R. Jones, C. J. W. Miles and P. S. Pusey.	Experiments in the Compressed Air Tunnel on swept-back wings including two delta wings. R. & M. 2871. March, 1948.
E9	—	German model tests.
E10	J. Trouncer and G. F. Moss ..	Low-speed tunnel tests on two 45-deg sweptback wings of aspect ratio, 4·5 and 3·0 (Models A and B). R. & M. 2710. June, 1947.
E11	R. Hills, R. C. Lock and J. G. Ross	Interim note on wind-tunnel tests of a model delta wing. A.R.C. 10,535. February, 1947. (Unpublished.)
E12	M. Gdaliahu	A summary of the results of some German model tests on wings of small aspect ratio. A.R.C. 9638. March, 1946. (Unpublished.)
E13	W. Jacobs	Pressure-distribution measurements on unyawed swept-back wings. Translation. N.A.C.A. Tech. Memo. 1164. July, 1947.
E14	V. M. Falkner	Calculated loadings due to incidence of a number of straight and swept-back wings. R. & M. 2596. June, 1948.
E15	A. Goodman and J. D. Brewer ..	Investigation at low speeds of the effect of aspect ratio and sweep on static and yawing stability derivatives of untapered wings. N.A.C.A. Tech. Note 1669. August, 1948.
E16	C. H. Zimmerman	Characteristics of Clark Y aerofoils of small aspect ratio. N.A.C.A. Report 431. 1932.
E17	H. Voepel	Tests on wings of small aspect ratio. R.A.E. Library Translation 276. October, 1948.

APPENDIX I

Geometrical Relations (see Fig. 15)

1. *Relations between a, δ, ω_0, ω_1.*—It follows from the definitions of a, δ that

$$a = \frac{\delta}{1 + \delta}$$

and from the geometry of Fig. 15 that

$$s' = \text{AD} \tan \omega_0 = a \,.\, \text{AD} \tan \omega_1$$

Hence

$$a = \frac{\delta}{1 + \delta} = \frac{\tan \omega_0}{\tan \omega_1} . \qquad \ldots \ldots \ldots \ldots \ldots \ldots \qquad (1)$$

2. *Aspect Ratio and Sweepback.*—If $\bar{c}$ is the mean chord, we have $A = 2s/\bar{c}$ and $\bar{c}/c_r = (1 + \lambda)/2$. Hence

$$A = \frac{4}{1 + \lambda} \frac{s}{c_r} = \frac{4}{1 + \lambda} \frac{s}{s'} \cdot \frac{s'}{c_r} .$$

But

$$\frac{s}{s'} = \frac{\text{BR}}{\text{BC}} = \frac{\text{AB} - \text{QR}}{\text{AB}} = 1 - \lambda$$

from similar triangles.

Also from triangle COD,

$$s' = \text{OD} \cot \phi_n = (1 - n + \delta) c_r \cot \phi_n$$

or

$$\frac{s'}{c_r} = (1 - n + \delta) \cot \phi_n .$$

Substituting for s/s' and s'/c_r in the expression for A we have

$$A \tan \phi_n = 4 \frac{1 - \lambda}{1 + \lambda} (1 - n + \delta) , \qquad \ldots \ldots \ldots \ldots \ldots \qquad (2)$$

ϕ_n being measured from the n-chord point.

It follows from (2) that ϕ_n vanishes when $\delta = n - 1$. For example, wings with no sweepback of the quarter-chord line correspond to $\delta = -\frac{3}{4}$.

3. *Formulae for Mean n-chord Points.*—Assume

(*a*) the local aerodynamic centre is at the n-chord point at every section

(*b*) the spanwise load L is $L_0 f(\eta)$, where L_0 is the lift per unit span at the centre and $\eta = y/s$.

The lift per unit span at section HK is therefore $L_0 f(\eta)$ and acts at P.

Then if $\bar{x}$ is the distance of the aerodynamic centre behind O we have

$$\bar{x} = \frac{\int_0^s x f(\eta)\, dy}{\int_0^s f(\eta)\, dy} = \frac{\int_0^s y \tan \phi_n f(\eta)\, dy}{\int_0^s f(\eta)\, dy}$$

$$= s \tan \phi_n \frac{\int_0^1 \eta f(\eta)\, d\eta}{\int_0^1 f(\eta)\, d\eta} .$$

But from the geometry of section 2

$$s \tan \phi_n = 2 \frac{1-\lambda}{1+\lambda}(1 - n + \delta)\bar{c}\,.$$

Hence

$$\frac{\bar{x}}{\bar{c}} = 2 \frac{1-\lambda}{1+\lambda}(1 - n + \delta) \frac{\int_0^1 \eta f(\eta)\, d\eta}{\int_0^1 f(\eta)\, d\eta}\,.$$

Finally if h is the distance of the aerodynamic centre behind the apex A, in terms of the mean chord, we have

$$h = \frac{2}{1+\lambda}\left\{ n + (1-\lambda)(1 - n + \delta) \frac{\int_0^1 \eta f(\eta)\, d\eta}{\int_0^1 f(\eta)\, d\eta} \right\}. \quad .. \quad .. \quad (3)$$

4. *Applications.*—(*a*) *Mean geometric n-chord point.*—In this case, which is usually taken to be the datum in aerodynamic centre analysis, the span load is proportional to the chord, *i.e.*,

$$f(\eta) = \frac{c}{c_r} = 1 - \eta(1-\lambda).$$

This gives

$$\frac{\int_0^1 \eta f(\eta)\, d\eta}{\int_0^1 f(\eta)\, d\eta} = \frac{\int_0^1 \left\{\eta - \eta^2(1-\lambda)\right\} d\eta}{\int_0^1 \left\{1 - \eta(1-\lambda)\right\} d\eta} = \frac{1+2\lambda}{3(1+\lambda)}\,.$$

Hence for the mean geometric n-chord point we have

$$h_{\text{geometric}} = \frac{2}{1+\lambda}\left\{ n + \frac{(1-\lambda)(1+2\lambda)}{3(1+\lambda)}(1 - n + \delta) \right\} \quad .. \quad .. \quad .. \quad (4)$$

and for the mean geometric quarter-chord point ($n = \frac{1}{4}$)

$$\left.\begin{aligned} h_{\text{geometric}} &= \frac{1}{2(1+\lambda)}\left\{1 + \frac{(1-\lambda)(1+2\lambda)}{1+\lambda}(1 + \tfrac{4}{3}\delta)\right\} \text{ in general} \\ &= 1 + \tfrac{2}{3}\delta \qquad \text{pointed tips } (\lambda = 0) \\ &= 1 \qquad\qquad\quad \text{delta } (\lambda = \delta = 0) \end{aligned}\right\} \quad .. \quad (5)$$

(*b*) *Mean elliptic n-chord point.*—In this case $f(\eta) = \sqrt{(1-\eta^2)}$, and putting $\eta = \sin\theta$,

$$\frac{\int_0^1 \eta f(\eta)\, d\eta}{\int_0^1 f(\eta)\, d\eta} = \frac{\int_0^{\pi/2} \sin\theta\, \cos^2\theta\, d\theta}{\int_0^{\pi/2} \cos^2\theta\, d\theta} = \frac{4}{3\pi}\,.$$

Hence for the mean elliptic n-chord point we have

$$h_{\text{elliptic}} = \frac{2}{1+\lambda}\left\{ n + \frac{4}{3\pi}(1-\lambda)(1 - n + \delta) \right\} \quad .. \quad .. \quad .. \quad .. \quad (6)$$

and for the mean elliptic quarter-chord point

$$\left.\begin{aligned} h_{\text{elliptic}} &= \frac{1}{2(1+\lambda)}\left\{1 + \frac{1-\lambda}{\pi}(4 + \tfrac{16}{3}\delta)\right\} \text{ in general} \\ &= 1{\cdot}136 + 0{\cdot}850\delta \quad \text{pointed tips } (\lambda = 0) \\ &= 1{\cdot}136 \qquad\qquad\quad \text{delta } (\lambda = \delta = 0) \end{aligned}\right\} \quad .. \quad .. \quad (7)$$

5. *Relative Positions of Geometric and Elliptic Points.*—Comparison of equations (2), (4) and (6) shows of course that the geometric and elliptic points coincide at zero sweepback, where $\delta = n - 1$. Moreover the δ slope of the geometric locus (equation (4)) is greater or less than that of the elliptic locus (equation (6)) according as

$$\frac{1 + 2\lambda}{1 + \lambda} \gtrless \frac{4}{\pi},$$

the dividing value being

$$\lambda = 0{\cdot}38 .$$

Hence for positive sweepback the mean geometric n-chord point will be in front of or behind the mean elliptic n-chord point according as the taper ratio is less or greater than 0·38. This is illustrated in Fig. 13.

APPENDIX II

Supersonic Spanwise and Chordwise Lift Distribution for Pointed Tips. External Solution (see Fig. 16)

1. The conical lift distribution is given by

$$\Delta p = C \frac{\tan^2 \omega_0}{\sqrt{(\tan^2 \omega_0 - \tan^2 \omega)}}$$

where the constant C is given by

$$C = \frac{4\alpha q}{E[\sqrt{(1 - k^2)}]} .$$

It is required to find the spanwise and chordwise lift distribution over the half-plan ABC shown in Fig. 16.

2. *Spanwise Loading.*—Referring to Fig. 16 let (x,y) be any point P of the section y whose end points are (x_0,y) and (x_1,y).

Introducing the variable $u = x \tan \omega_0$, and noting that $y = x \tan \omega$, we have $u_0 = y$ at H and $u_1 = x_1 \tan \omega_0$ at K.

With this substitution

$$\Delta p = \frac{Cx \tan^2 \omega_0}{\sqrt{(u^2 - y^2)}} .$$

Hence if L be the lift per unit span at the section y, then

$$\begin{aligned} L &= \int_{x_0}^{x_1} \Delta p \, dx \\ &= C \int_y^{u_1} \frac{u \, du}{\sqrt{(u^2 - y^2)}} = C \left[\sqrt{(u^2 - y^2)}\right]_y^{u_1} \\ &= C\sqrt{(u_1^2 - y^2)} . \qquad \ldots \ldots \ldots \ldots \ldots \ldots \quad (1) \end{aligned}$$

Now

$$\begin{aligned} u_1 &= x_1 \tan \omega_0 \\ &= \tan \omega_0 \, (c_r + y \cot \omega_1) \end{aligned}$$

and

$$c_r = s(\cot \omega_0 - \cot \omega_1) .$$

Hence $$u_1 = s \tan \omega_0 (\cot \omega_0 - \cot \omega_1) + y \tan \omega_0 \cot \omega_1$$
$$= s\{(1 - \tan \omega_0 \cot \omega_1) + \eta \tan \omega_0 \cot \omega_1\}$$

where $$\eta = y/s .$$

But $$\tan \omega_0 \cot \omega_1 = \frac{\delta}{1+\delta},$$

and so $$\frac{u_1}{s} = 1 - \frac{\delta}{1+\delta} + \frac{\delta}{1+\delta}\eta = \frac{1+\delta\eta}{1+\delta}.$$

Substituting in (1) we have

$$L = Cs\sqrt{\left[\left(\frac{1+\delta\eta}{1+\delta}\right)^2 - \eta^2\right]}.$$

Also if $L = L_0$ at $\eta = 0$, then

$$L_0 = \frac{Cs}{1+\delta}.$$

Thus for the span loading $f(\eta) = L/L_0$ we have

$$f = \sqrt{[(1+\delta\eta)^2 - \eta^2(1+\delta)^2]}$$
$$= \sqrt{[(1-\eta^2) + 2\delta(\eta - \eta^2)]}. \quad .. \quad .. \quad .. \quad .. \quad (2)$$

This shows that the spanwise loading of the delta is elliptic, but that arrow-heads are loaded super-elliptically and lozenges sub-elliptically, the departure being represented by the additional term $2\delta(\eta - \eta^2)$.

The span loading is plotted in Fig. 8 for a range of δ from $-0{\cdot}5$ to 4.

3. *Chordwise Loading—Local Aerodynamic Centre.*—Let the local aerodynamic centre at the section y be at the n_l-chord point.

Then taking moments about H

$$n_l = \frac{\int_{x_0}^{x_1} (x - x_0)\, \Delta p\, dx}{(x_1 - x_0)\int_{x_0}^{x_1} \Delta p\, dx}$$

$$= \frac{\int_{u_0}^{u} \frac{u(u-u_0)}{\sqrt{(u^2 - y^2)}}\, du}{(u_1 - u_0)\int_{u_0}^{u_1} \frac{u\, du}{\sqrt{(u^2 - y^2)}}}$$

$$= \frac{I_1 - u_0 I_0}{(u_1 - u_0) I_0} \quad .. \quad .. \quad .. \quad .. \quad .. \quad .. \quad .. \quad (3)$$

where $$I_0 = \int_{u_0}^{u_1} \frac{u\, du}{\sqrt{(u^2 - y^2)}} = \sqrt{(u_1^2 - y^2)}$$

and $$I_1 = \int_{u_0}^{u_1} \frac{u^2\, du}{\sqrt{(u^2 - y^2)}}.$$

Now
$$\int \frac{u^2\,du}{u^2-y^2} = u\sqrt{(u^2-y^2)} - \int \sqrt{(u^2-y^2)}\,du$$
$$= \frac{u}{2}\sqrt{(u^2-y^2)} + \frac{y^2}{2}\log\,(u+\sqrt{(u^2-y^2)})$$

and so
$$I_1 = \frac{u_1}{2}\sqrt{(u_1^2-y^2)} + \frac{y^2}{2}\log\,(u_1+\sqrt{(u_1^2-y^2)})\,.$$

Substituting for I_0, I_1 in (3) and reducing we have

$$n_l = \tfrac{1}{2} - \frac{u_0}{2(u_1-u_0)} + \frac{y^2}{2(u_1-u_0)\sqrt{(u_1^2-y^2)}}\log\frac{u_1+\sqrt{(u_1^2-y^2)}}{u_0} \quad \ldots\ldots \quad (4)$$

In order to express this in terms of δ and η we note from section 2 that

$$\frac{u_0}{s} = \eta \quad \text{and} \quad \frac{u_1}{s} = \frac{1+\delta\eta}{1+\delta}\,.$$

Substituting in (4) and reducing we have finally :—

$$n_l = \tfrac{1}{2} - \frac{(1+\delta)\eta}{2(1-\eta)} + \frac{(1+\delta)^2\eta^2}{2(1-\eta)\sqrt{[1+2\delta\eta-(1+2\delta)\eta^2]}}\log\left[\frac{1+\delta\eta+\sqrt{[1+2\delta\eta-(1+2\delta)\eta^2]}}{(1+\delta)\eta}\right]. \quad (5)$$

It is easily seen that $n_l \to \frac{1}{2}$ as $\eta \to 0$.

The limit as $\eta \to 1$ is more difficult to find. Putting $\eta = 1 - \varepsilon$ where ε is small, the log term reduces to

$$\sqrt{\left(\frac{2\varepsilon}{1+\delta}\right)}\cdot\left\{1+\frac{\varepsilon}{1+\delta}\,\frac{(6\delta+5)}{12}\right\} \text{ up to } \varepsilon^{3/2}\,.$$

The multiplier of the log term reduces to

$$\frac{1}{\sqrt{\left(\frac{2\varepsilon}{1+\delta}\right)}}\cdot\frac{(1-\varepsilon)^2}{2\varepsilon}(1+\delta)\left(1+\frac{\varepsilon}{4}\cdot\frac{1+2\delta}{1+\delta}\right).$$

The whole expression for n_l may then be written

$$n_l = \tfrac{1}{2} - \frac{1-\varepsilon}{2\varepsilon}(1+\delta) + \frac{(1-\varepsilon)^2}{2\varepsilon}(1+\delta)\left[1+\frac{\varepsilon}{4}\,\frac{1+2\delta}{1+\delta}\right]\left[1+\frac{\varepsilon(6\delta+5)}{12(1+\delta)}\right]$$

and this reduces to

$$n_l = \tfrac{1}{3} + O(\varepsilon)\,.$$

Hence $n_l \to \frac{1}{3}$ as $\eta \to 1$.

In Fig. 9 n_l is plotted against η for values of δ between $-\frac{1}{2}$ and 4. Comparing this with the spanwise loading of Fig. 8, it appears that

(*a*) While the spanwise loading of a delta is elliptic, its local aerodynamic centre is forward of the half-chord point, and so its aerodynamic centre will be forward of the mean elleptic half-chord point (*see* Fig. 7). The appropriate value of n is in fact 0·42.

(*b*) When δ is positive the span loading becomes super-elliptic but the local aerodynamic centre moves forward, and conversely when δ is negative. These effects tend to cancel in such a way as to leave the mean elliptic 0·45-point ($n = 0{\cdot}45$) a fair approximation to the aerodynamic centre between $\delta = -\frac{1}{2}$ and $1\frac{1}{2}$ (Fig. 7).

(*c*) For $\delta > 1{\cdot}5$ the super-elliptic loading predominates and moves the aerodynamic centre more and more aft of the mean elliptic half-chord point as δ increases. A rough approximation is $n = 0{\cdot}61$ between $\delta = 1{\cdot}5$ and 4 (Fig. 7).

TABLE I.
TAPERED WINGS.

POINT	REFERENCE	δ	λ	A	$\phi_{1/4}$	$R/10^6$	SECTION ROOT	SECTION TIP	β	βA	TAN ϕ/β	MEASURED a.c. $H_{SUBSONIC}$	SUBSONIC REFERENCE PTS. GEOM. 1/4	SUBSONIC REFERENCE PTS. ELLIPTIC 1/4	THEORETICAL a.c. $H_{SUPERSONIC}$ ELLIPTIC 0·4 S	TRANSONIC a.c. MOVEMENT $H_{SUPERSONIC}$ $H_{SUBSONIC}$
1	1	−0·82	0·24	6·47	−2·0	1·1	Modified Piercy-1·75% camber @ 0·3c 12·5% 1/c @ 0·35 c	10% 1/c @ 0·35 c	≈1·0	≈ A	−0·035	0·367	0·369	0·373	0·586	0·22
2	1	−0·82	0·24	6·47	−2·0	1·1	Modified Piercy-1·75% camber @ 0·3c 12·5% 1/c @ 0·35c	10% 1/c @ 0·35 c	0·69	4·464	−0·051	0·297	0·369	0·373	0·586	0·29
3	6	−0·75	0	3·0	0	1·2	FLAT PLATE	FLAT PLATE	≈1·0	≈ A	0	0·435	0·50	0·5	0·730*	0·30*
4	2	−0·75	0·2	10·0	0	6·5	NACA 23016	NACA 23009	≈1·0	≈ A	0	0·406	0·417	0·417	0·635	0·23
5	2	−0·75	0·2	10·0	0	6·5	NACA 23018	NACA 23009	≈1·0	≈ A	0	0·404	0·417	0·417	0·635	0·23
6	5	−0·75	0·2	10·6	0	2·56	NACA 654-020	NACA 653-018	≈1·0	≈ A	0	0·449	0·417	0·417	0·635	0·19
7	2	−0·75	0·2	12·0	0	6·5	NACA 23016	NACA 23009	≈1·0	≈ A	0	0·401	0·417	0·417	0·635	0·23
8	2	−0·75	0·2	12·0	0	6·5	NACA 23020	NACA 23009	≈1·0	≈ A	0	0·407	0·417	0·417	0·635	0·23
9	2	−0·75	0·333	10·0	0	6·7	NACA 23018	NACA 23009	≈1·0	≈ A	0	0·362	0·375	0·375	0·588	0·23
10	5	−0·75	0·5	3·0	0	0·31	RHODE ST. GENESE 35	RHODE ST. GENESE 35	≈1·0	≈ A	0	0·309	0·333	0·333	0·600	0·29
11	3	−0·75	0·5	6·0	0	4·6	+ NACA 65_2-215	+ NACA 65_2-215	≈1·0	≈ A	0	0·345	0·333	0·333	0·600	0·26
12	3	−0·75	0·5	6·0	0	11·7	+ NACA 65_2-215	+ NACA 65_2-215	0·71	4·26	0	0·341	0·333	0·333	0·600	0·26
13	5	−0·75	0·5	6·0	0	3·09	NACA 24 SERIES	NACA 24 SERIES	≈1·0	≈ A	0	0·315	0·333	0·333	0·600	0·29
14	4	−0·75	0·6	5·8	0	1·2	§ MAX. t/c = 0·14	§ MAX. t/c = 0·14	0·80	4·64	0	0·287	0·313	0·313	0·530	0·24
15	2	−0·75	0·625	6·0	0	8·18	NACA 23013	NACA 43010	≈1·0	≈ A	0	0·287	0·308	0·308	0·576	0·29
16	7	−0·74	0·417	5·1	1·9	4·7	0·14 1/c MAX @ 0·4 c	0·11 1/c MAX @ 0·4 c	0·91	4·64	0·037	0·336	0·356	0·356	0·590	0·25
17	7	−0·74	0·417	5·1	1·9	4·7	0·14 1/c MAX @ 0·4c	0·11 1/c MAX @ 0·4 c	0·68	3·468	0·049	0·326	0·356	0·356	0·590	0·26
18	6	−0·50	0·2	6·0	6·34	1·2	NACA 23012	NACA 23012	≈1·0	≈ A	0·110	0·562	0·546	0·558	0·780	0·22
19	2	−0·08	0·25	6·0	15·0	6·5	NACA 0015	NACA 0009	≈1·0	≈ A	0·268	0·734	0·722	0·742	0·960	0·23
20	12	0	0	1·0	18·4	2·0	NACA 0012	NACA 0012	≈1·0	≈ A	0·333	1·220	1·0	1·136	1·366*	0·15*
21	12	0	0	1·33	23·9	2·0	NACA 0012	NACA 0012	≈1·0	≈ A	0·443	1·190	1·0	1·136	1·366*	0·18*
22	12	0	0	2·0	33·7	2·0	NACA 0012	NACA 0012	≈1·0	≈ A	0·667	1·168	1·0	1·136	1·366*	0·20*
23	8	0	0	2·31	37·6	8·0	SQUIRE H.S. 'C'	SQUIRE H.S. 'C'	≈1·0	≈ A	0·770	1·160	1·0	1·136	1·366*	0·21*
24	12	0	0	3·0	45·0	2·0	NACA 0012	NACA 0012	≈1·0	≈ A	1·0	1·120	1·0	1·136	1·366*	0·24*
25	8	0	0	3·87	52·2	8·0	SQUIRE H.S. 'C'	SQUIRE H.S. 'C'	≈1·0	≈ A	1·289	1·100	1·0	1·136	1·366*	0·27*
26	11	0	0	4·0	53·1	2·7	SQUIRE H.S. 'C'	SQUIRE H.S. 'C'	≈1·0	≈ A	1·332	1·115	1·0	1·136	1·366*	0·25*
27	8	0	0·12	3·04	35·3	8·0	SQUIRE H.S. 'C'	SQUIRE H.S. 'C'	≈1·0	≈ A	0·708	0·935	0·877	0·947	1·227	0·29
28	12	0	0·125	1·35	17·1	2·0	NACA 0012	NACA 0012	≈1·0	≈ A	0·308	0·990	0·877	0·938	1·165	0·17
29	11	0	0·136	3·0	39·9	2·4	SQUIRE H.S. 'C'	SQUIRE H.S. 'C'	≈1·0	≈ A	0·836	0·943	0·872	0·922	1·148	0·21
30	8	0	0·23	2·38	23·4	8·0	SQUIRE H.S. 'C'	SQUIRE H.S. 'C'	≈1·0	≈ A	0·433	0·785	0·780	0·805	1·025	0·24
31	12	0	0·25	1·33	14·9	2·0	NACA 0012	NACA 0012	≈1·0	≈ A	0·266	0·810	0·758	0·733	1·0	0·19
32	11	0	0·268	2·31	24·0	2·1	SQUIRE H.S. 'C'	SQUIRE H.S. 'C'	≈1·0	≈ A	0·445	0·780	0·745	0·761	0·981	0·20
33	6	0	0·333	6·0	14·04	1·2	NACA 23012	NACA 23012	≈1·0	≈ A	0·249	0·677	0·688	0·683	0·908	0·23
34	12	0	0·5	1·33	8·4	2·0	NACA 0012	NACA 0012	≈1·0	≈ A	0·148	0·557	0·556	0·545	0·757	0·20
35	8	0·28	0·25	3·07	45·0	8·0	SQUIRE H.S. 'C'	SQUIRE H.S. 'C'	≈1·0	≈ A	1·0	0·970	0·892	0·925	1·143	0·06
36	3	0·41	0·5	5·76	15·0	4·6	+ NACA 65_2-215	+ NACA 65_2-215	≈1·0	≈ A	0·268	0·679	0·677	0·662	0·873	0·19
37	3	0·41	0·5	5·76	15·0	11·9	+ NACA 65_2-215	+ NACA 65_2-215	0·71	4·09	0·378	0·692	0·677	0·662	0·873	0·18
38	5	0·46	0·5	6·0	15·0	3·10	NACA 24 SERIES	NACA 24 SERIES	≈1·0	≈ A	0·268	0·677	0·691	0·675	0·885	0·21
39	10	0·50	0·25	3·0	45·0	1·5	SQUIRE H.S. 'B'	SQUIRE H.S. 'B'	≈1·0	≈ A	1·0	1·090	1·0	1·037	1·253	0·16
40	6	0·93	0·49	3·0	37·5	1·2	# NACA 23012	# NACA 23012	≈1·0	≈ A	0·767	0·866	0·845	0·824	1·038	0·17
41	6	1·07	0·408	2·08	55·8	1·2	# NACA 23012	# NACA 23012	≈1·0	≈ A	1·472	1·097	1·012	1·005	1·138	0·04
42	9	1·125	0·2	5·0	45·0	—	—	—	≈1·0	≈ A	1·0	1·380	1·39	1·423	1·695	0·32
43	10	1·125	0·25	4·5	45·0	1·5	SQUIRE H.S. 'B'	SQUIRE H.S. 'B'	≈1·0	≈ A	1·0	1·390	1·30	1·355	1·573	0·18
44	3	1·315	0·499	4·78	30·0	5·0	+ NACA 65_2-215	+ NACA 65_2-215	≈1·0	≈ A	0·577	0·970	0·943	0·917	1·129	0·16
45	3	1·315	0·499	4·78	30·0	13·1	+ NACA 65_2-215	+ NACA 65_2-215	0·71	3·514	0·813	0·982	0·943	0·917	1·129	0·15
46	4	1·36	0·6	5·8	20·0	1·2	§ MAX. t/c = 0·14	§ MAX. t/c = 0·14	0·80	4·64	0·455	0·788	0·796	0·761	0·967	0·18
47	4	1·67	0·25	5·8	45·0	1·2	§ MAX. t/c = 0·14	§ MAX. t/c = 0·14	0·80	4·64	1·25	1·678	1·560	1·631	1·850	0·17
48	3	1·72	0·497	3·32	45·0	6·1	+ NACA 65_2-215	+ NACA 65_2-215	≈1·0	≈ A	1·0	1·133	1·072	1·039	1·247	0·11
49	3	1·72	0·497	3·32	45·0	15·8	+ NACA 65_2-215	+ NACA 65_2-215	0·71	2·357	1·406	1·133	1·072	1·039	1·247	0·11
50	5	1·85	0·5	6·0	30·0	3·09	NACA 24 SERIES	NACA 2409	≈1·0	≈ A	0·577	1·111	1·103	1·069	1·277	0·17
51	5	1·85	0·5	6·0	30·0	8·16	WING TIP TWIST 8 1/2° NACA 2415	NACA 2409	≈1·0	≈ A	0·577	1·112	1·103	1·069	1·277	0·17
52	5	2·40	0·5	6·0	35·0	2·0	NACA 0012-1130 (MODIFIED	NACA 0012)	≈1·0	≈ A	0·700	1·284	1·263	1·223	1·458	0·15
53	5	3·19	0·5	5·84	42·0	0·22	RHODE ST. GENESE 33	RHODE ST. GENESE 33	≈1·0	≈ A	0·900	1·557	1·502	1·449	1·660	0·10
54	4	3·311	0·6	5·8	35·0	1·2	§ MAX. t/c = 0·14	§ MAX. t/c = 0·14	0·80	4·64	0·875	1·261	1·243	1·172	1·390	0·13
55	4	5·05	0·6	5·8	45·0	1·2	§ MAX. t/c = 0·14	§ MAX. t/c = 0·14	0·80	4·64	1·25	1·660	1·642	1·543	1·748	0·09

* $H_{SUPERSONIC}$ IS UNCONFIRMED BY THEORY EXCEPT FOR λ=0, AT WHICH THE RESULTS ARE STARRED.

\# SECTION PERPENDICULAR TO TRAILING EDGE.

\+ SECTION PERPENDICULAR TO 1/4 CHORD.

§ SCALED UP SQUIRE H.S. 'B' SECTION (MAX. t/c = 0·10).

NUMBER	REFERENCE
E 1	RAE REPORT No AERO 2000.
2	NACA TECH. REPORT No 627.
3	NACA TECH. NOTE No 1709.
4	R A E REPORT No AERO 2295.
5	NACA TECH. NOTE No 1095.
6	NACA RM NACA/TIB/1352.
7	R A E REPORT No AERO 2061.
8	A R C REPORT No 11,354.
9	GERMAN TESTS.
10	R A E REPORT No AERO 2210.
11	R A E TECH. NOTE No AERO 1869.
12	R A E TECH. NOTE No AERO 1767.

TABLE 2.

UNTAPERED WINGS.

	POINT.	REF.	γ	A	ϕ	SECTION. ROOT	SECTION. TIP	$R/10^6$	β	βA	$\frac{\tan\phi}{\beta}$	H SUBSONIC	MEAN GEOM $\frac{t}{4}$	MEAN ELLIPTIC $\frac{t}{4}$
	1	17	0	0·5	0	NACA0012	NACA0009	1·18	≈ 1·0	≈ A	0	0·14	0·25	0·25
☼	2	14	0	1·0	0	FLAT PLATE.		–	≈ 1·0	≈ A	0	0·148	0·25	0·25
	3	16	0	1·0	0	CLARK Y	CLARK Y	0·86	≈ 1·0	≈ A	0	0·203	0·25	0·25
	4	17	0	1·0	0	NACA0012	NACA0009	0·83	≈ 1·0	≈ A	0	0·18	0·25	0·25
	5	6	0	1·27	0	FLAT PLATE	FLAT PLATE	≈1·2	≈ 1·0	≈ A	0	0·185	0·25	0·25
	6	15	0	1·34	0	NACA0012	NACA0012	1·58	≈ 1·0	≈ A	0	0·184	0·25	0·25
☼	7	14	0	2·0	0	FLAT PLATE		–	≈ 1·0	≈ A	0	0·211	0·25	0·25
	8	17	0	2·0	0	NACA0012	NACA0009	0·59	≈ 1·0	≈ A	0	0·20	0·25	0·25
	9	15	0	2·61	0	NACA0012	NACA0012	1·10	≈ 1·0	≈ A	0	0·193	0·25	0·25
	10	6	0	3·0	0	FLAT PLATE	FLAT PLATE	≈1·2	≈ 1·0	≈ A	0	0·239	0·25	0·25
	11	6	0	3·0	0	NACA0012	NACA0012	≈1·2	≈ 1·0	≈ A	0	0·239	0·25	0·25
	12	16	0	3·0	0	CLARK Y	CLARK Y	0·86	≈ 1·0	≈ A	0	0·230	0·25	0·25
	13	6	0	3·0	0	NACA0015	NACA0015	≈1·2	≈ 1·0	≈ A	0	0·227	0·25	0·25
☼	14	14	0	4·0	0	FLAT PLATE.		–	≈ 1·0	≈ A	0	0·230	0·25	0·25
	15	13	0	5·0	0	NACA23012	NACA23012	0·42	≈ 1·0	≈ A	0	0·25	0·25	0·25
	16	15	0	5·16	0	NACA0012	NACA0012	0·78	≈ 1·0	≈ A	0	0·200	0·25	0·25
	17	6	0	6·0	0	NACA0015	NACA0015	≈1·2	≈ 1·0	≈ A	0	0·245	0·25	0·25
☼	18	14	0	6·0	0	FLAT PLATE.		–	≈ 1·0	≈ A	0	0·24	0·25	0·25
	19	16	0	6·0	0	CLARK Y	CLARK Y	0·86	≈ 1·0	≈ A	0	0·223	0·25	0·25
	20	6	0	6·0	0	NACA0012	NACA0012	≈1·2	≈ 1·0	≈ A	0	0·220	0·25	0·25
☼	21	14	0·289	1·0	30	FLAT PLATE		–	≈ 1·0	≈ A	0·5774	0·287	0·395	0·25
☼	22	14	0·500	1·0	45	FLAT PLATE		–	≈ 1·0	≈ A	1·0	0·405	0·5	0·462
☼	23	14	0·5785	2·0	30	FLAT PLATE		–	≈ 1·0	≈ A	0·5774	0·469	0·539	0·495
	24	13	0·67	5·0	15	NACA23012	NACA23012	0·42	≈ 1·0	≈ A	0·2680	0·565	0·585	0·534
☼	25	14	1·0	2·0	45	FLAT PLATE		–	≈ 1·0	≈ A	1·0	0·676	0·75	0·674
	26	5	1·05	2·5	40	NACA0012	NACA0012	0·63	≈ 1·0	≈ A	0·8391	0·773	0·774	0·695
☼	27	14	1·16	4·0	30	FLAT PLATE		–	≈ 1·0	≈ A	0·5774	0·762	0·83	0·742
	28	5	1·28	4·36	30	NACA23012	NACA23012	1·1	≈ 1·0	≈ A	0·5774	0·833	0·879	0·784
	29	6	1·295	1·49	60	NACA0012	NACA0012	≈1·2	≈ 1·0	≈ A	1·7321	0·855	0·895	0·798
	30	6	1·3	1·5	60	NACA0015	NACA0015	≈1·2	≈ 1·0	≈ A	1·7321	0·845	0·899	0·801
	31	6	1·3	4·5	30	NACA0015	NACA0015	≈1·2	≈ 1·0	≈ A	0·5774	0·830	0·900	0·801
	32	13	1·445	5·0	30	NACA23012	NACA23012	0·42	≈ 1·0	≈ A	0·5774	0·940	0·972	0·863
	33	6	1·5	5·2	30	NACA0015	NACA0015	≈1·2	≈ 1·0	≈ A	0·5774	0·931	1·001	0·887
	34	5	1·675	4·0	40	NACA0012	NACA0012	0·63	≈ 1·0	≈ A	0·8391	1·115	1·089	0·962
☼	35	14	1·73	6·0	30	FLAT PLATE.		–	≈ 1·0	≈ A	0·5774	1·053	1·115	0·984
	36	5	1·78	3·56	45	NACA23012	NACA23012	1·37	≈ 1·0	≈ A	1·0	1·089	1·140	1·005
☼	37	14	2·0	4·0	45	FLAT PLATE		–	≈ 1·0	≈ A	1·0	1·182	1·25	1·10
	38	5	2·05	4·1	45	NACA23012	NACA23012	1·37	≈ 1·0	≈ A	1·0	1·215	1·275	1·120
	39	6	2·27	2·62	60	NACA0012	NACA0012	≈1·2	≈ 1·0	≈ A	1·7321	1·345	1·385	1·213
	40	13	2·5	5·0	45	NACA23012	NACA23012	0·42	≈ 1·0	≈ A	1·0	1·460	1·5	1·311
	41	6	2·6	3·0	60	NACA0015	NACA0015	≈1·2	≈ 1·0	≈ A	1·7321	1·494	1·549	1·353
	42	6	2·72	3·14	60	NACA0012	NACA0012	≈1·2	≈ 1·0	≈ A	1·7321	1·680	1·610	1·404
☼	43	14	3·0	6·0	45	FLAT PLATE.		–	≈ 1·0	≈ A	1·0	1·697	1·75	1·663

REFERENCES

5 NACA TECH. NOTE. 1093.

6 NACA REP. RM. L7. D23.

15 NACA TECH. MEMO. 1164

☼ 14 ARC 11,542 (CALCULATED)

15 NACA TECH NOTE. 1669.

16 NACA REP Nº 431

17 R.A.E. LIBRARY TRANS. 276

+ SECTION NORMAL TO LEADING EDGE.

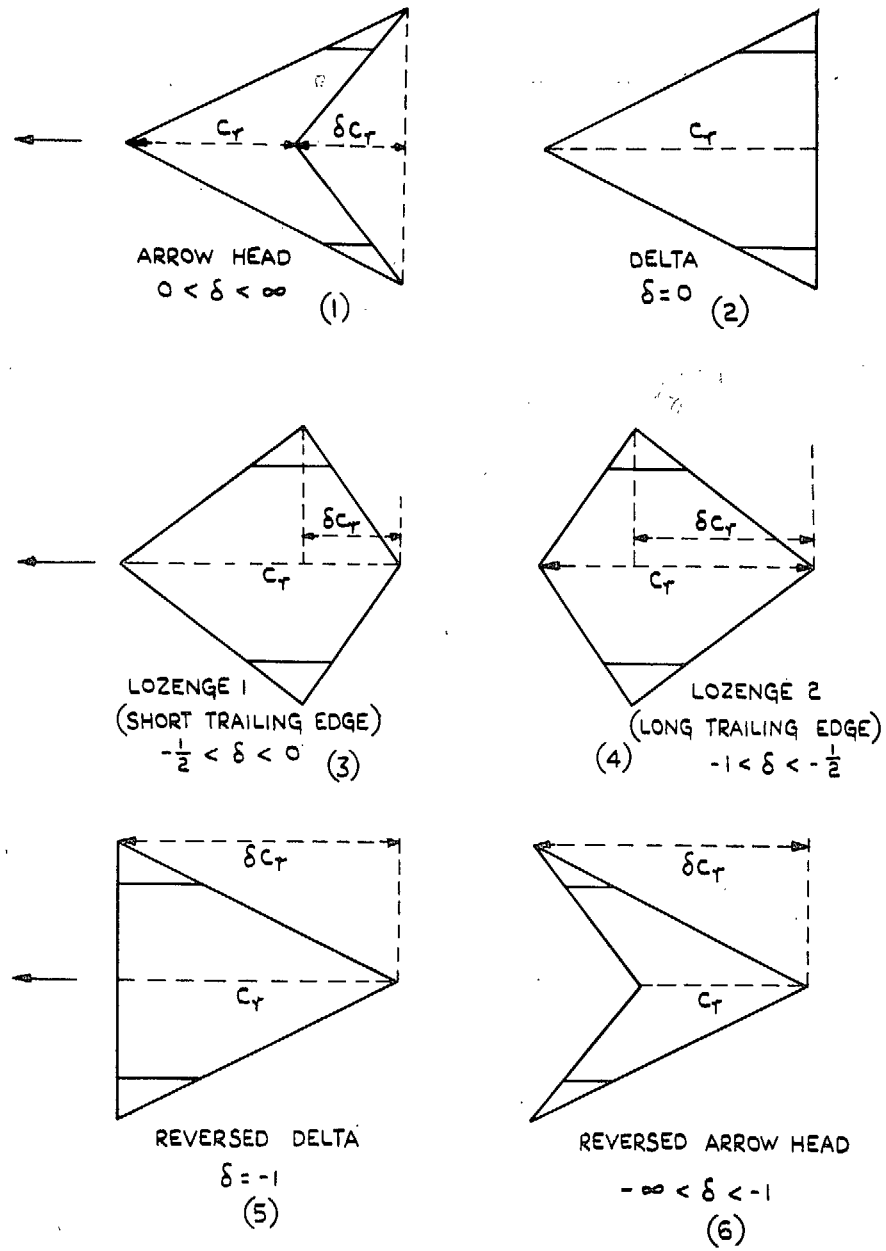

FIG. 1. Plan-form classification according to δ.

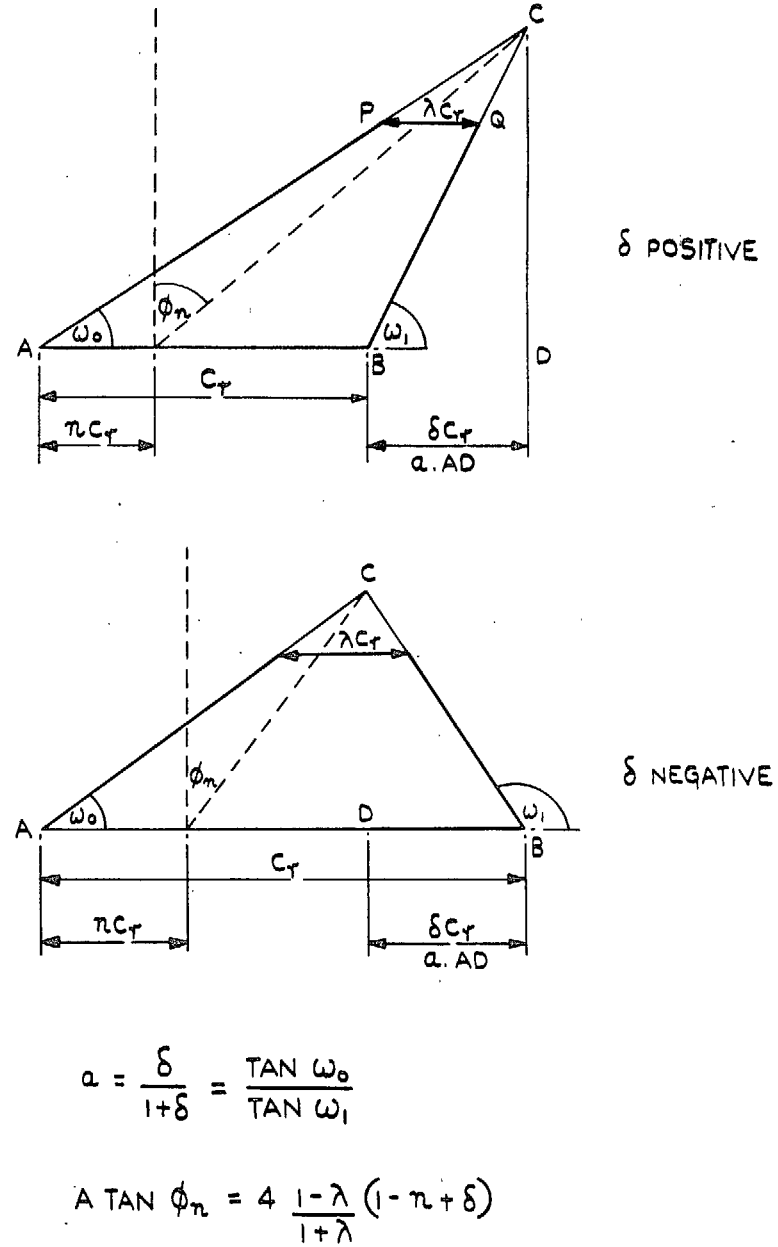

$$a = \frac{\delta}{1+\delta} = \frac{\text{TAN } \omega_0}{\text{TAN } \omega_1}$$

$$A \text{ TAN } \phi_n = 4 \frac{1-\lambda}{1+\lambda} (1 - n + \delta)$$

FIG. 2. Geometrical definitions for the δ analysis.

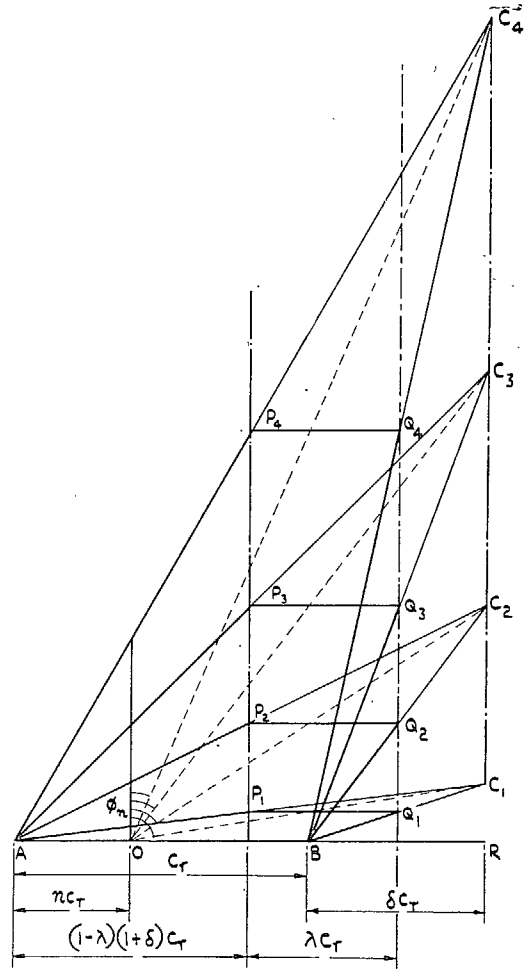

THE SHAPE IS DEFINED BY δ, λ, ϕ_n

THE ASPECT RATIO A IS GIVEN BY

$$A \tan \phi_n = 4 \frac{1-\lambda}{1+\lambda} (1 - n + \delta)$$

TWO FAMILIES ARE SHOWN (a) TRIANGLES ABC$_1$ ETC. $(\lambda = 0)$

(b) TRAPEZIA ABQ$_1$P$_1$ ETC. $(\lambda = \frac{1}{2})$

FIG. 3. Families of half-plans at constant δ and λ.

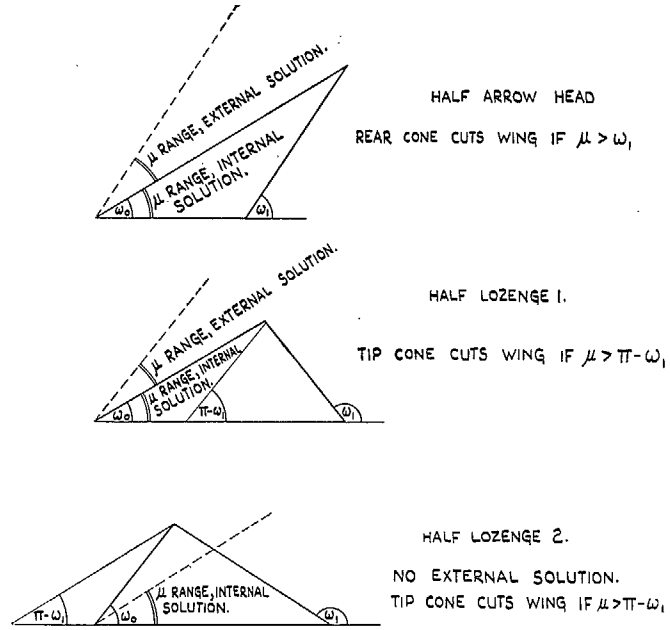

FIG. 4. Mach angle ranges for external and internal supersonic solution.

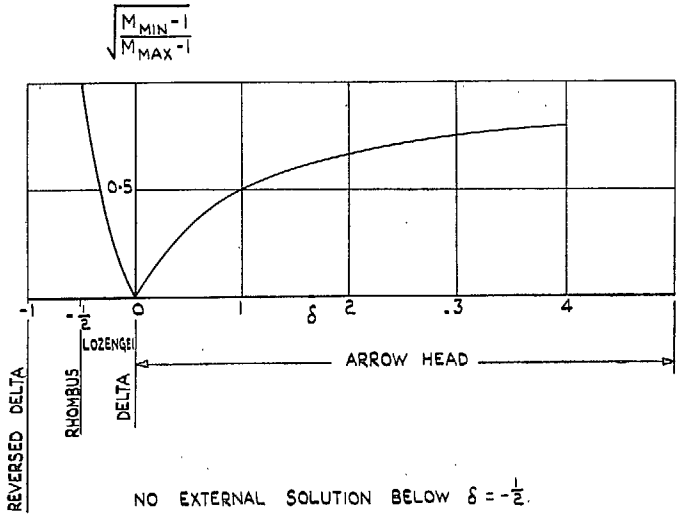

FIG. 5. Relation between limiting Mach numbers, $M_{\min}$, $M_{\max}$ for external solution.

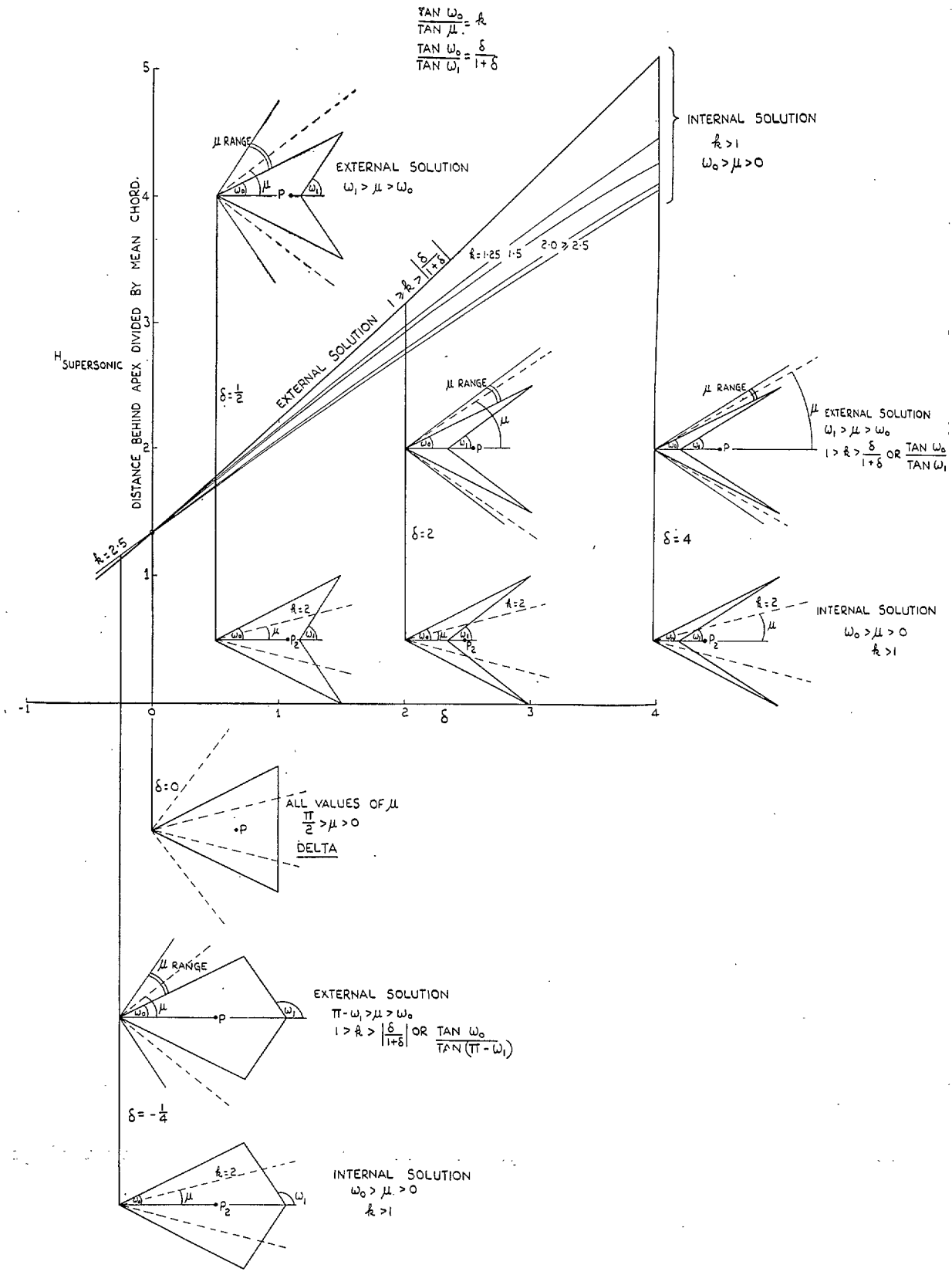

FIG. 6. Aerodynamic centre for conical flow with pointed tips.

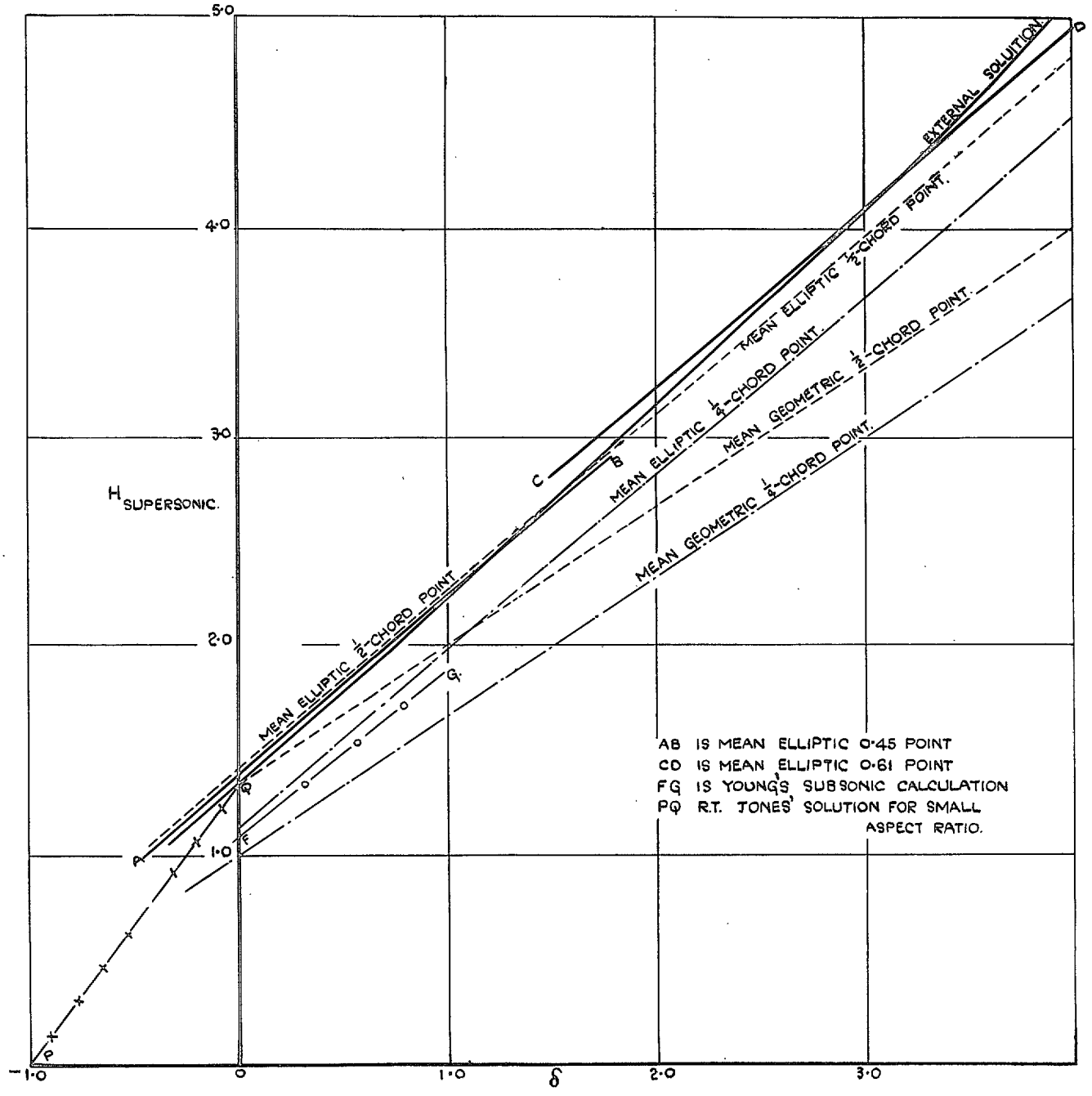

FIG. 7. Approximations to the external supersonic solution for aerodynamic centre with pointed tips.

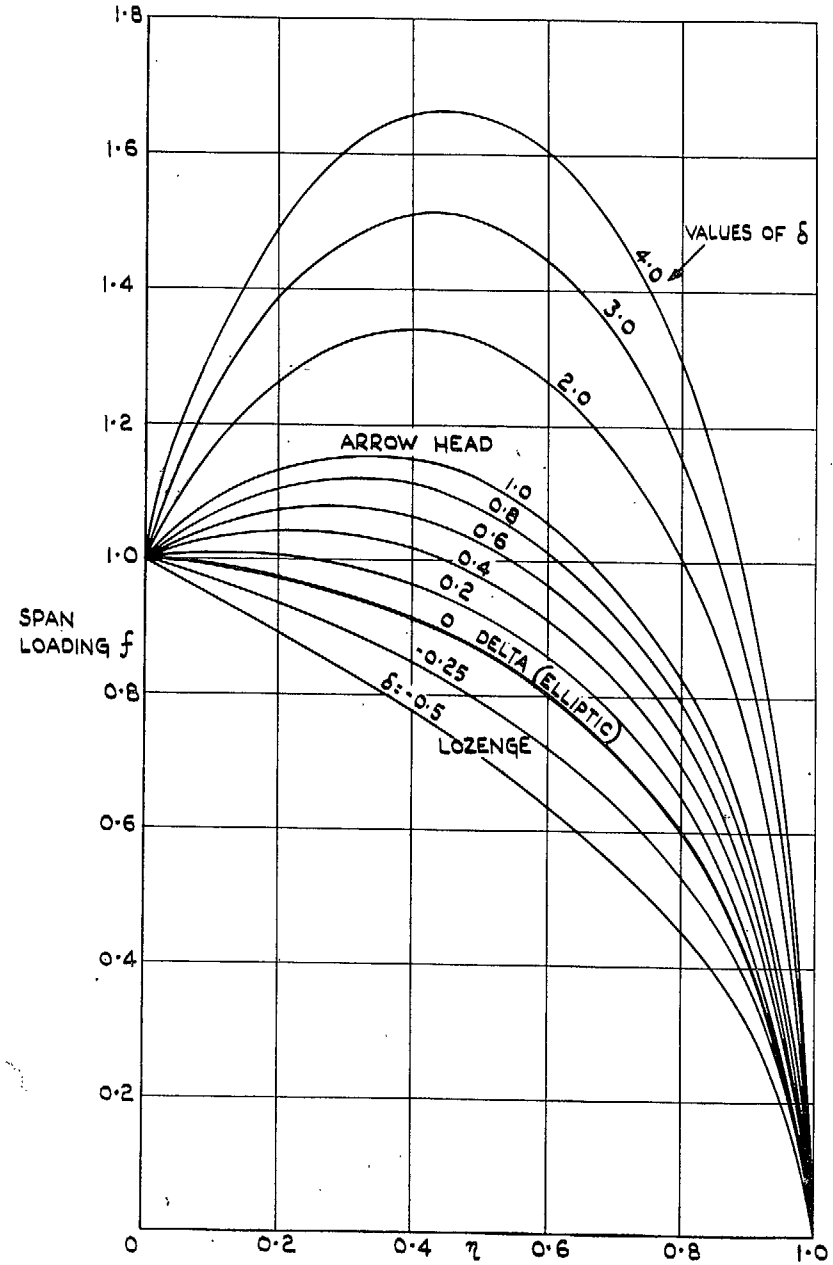

FIG. 8. Supersonic spanwise loading of pointed wings, external solution.

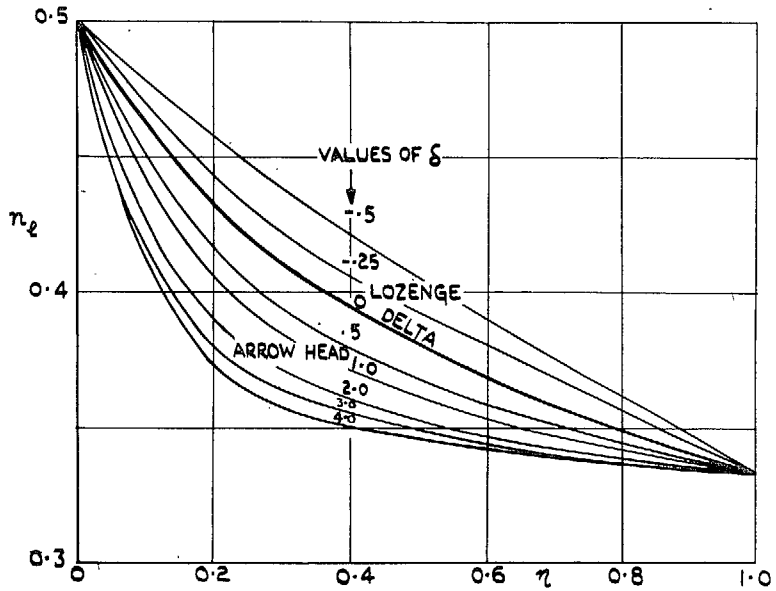

FIG. 9. Supersonic chordwise lift distribution for pointed wings, external solution. n_l is distance of local aerodynamic centre behind the nose of the local chord, in terms of the local chord.

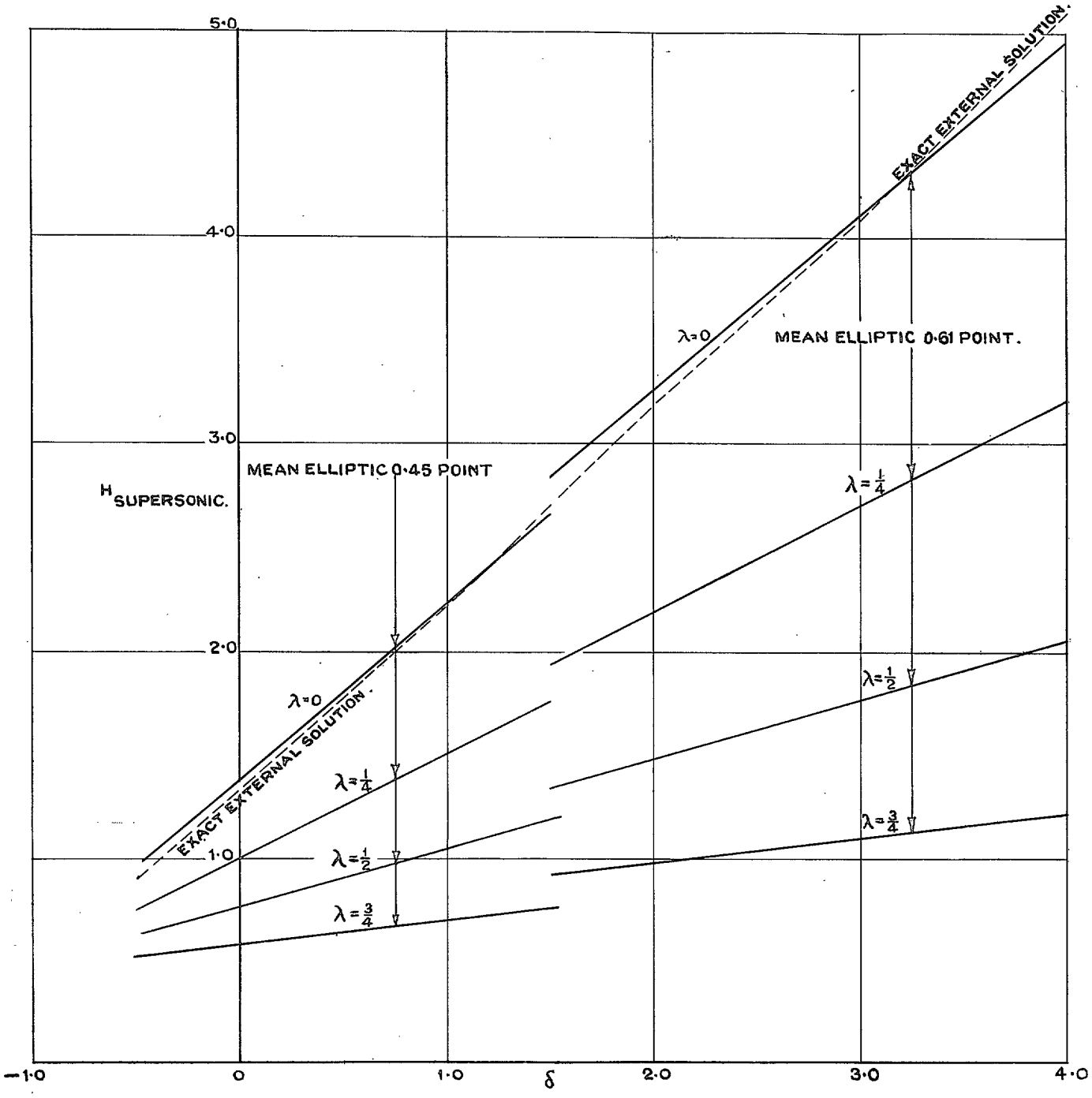

FIG. 10. Rough approximation to supersonic aerodynamic centre for finite taper ratio λ. External solution.

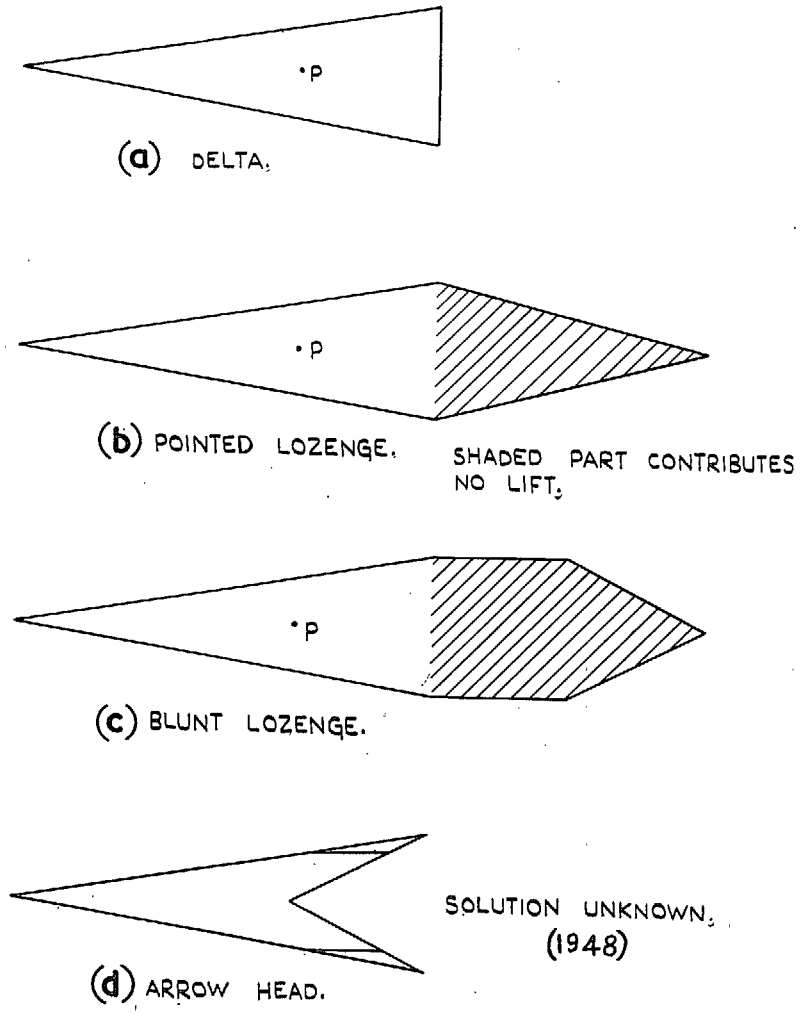

FIGS. 11a, 11b, 11c and 11d. Aerodynamic centre P of slender pointed wings. (R. T. Jones's theory.)

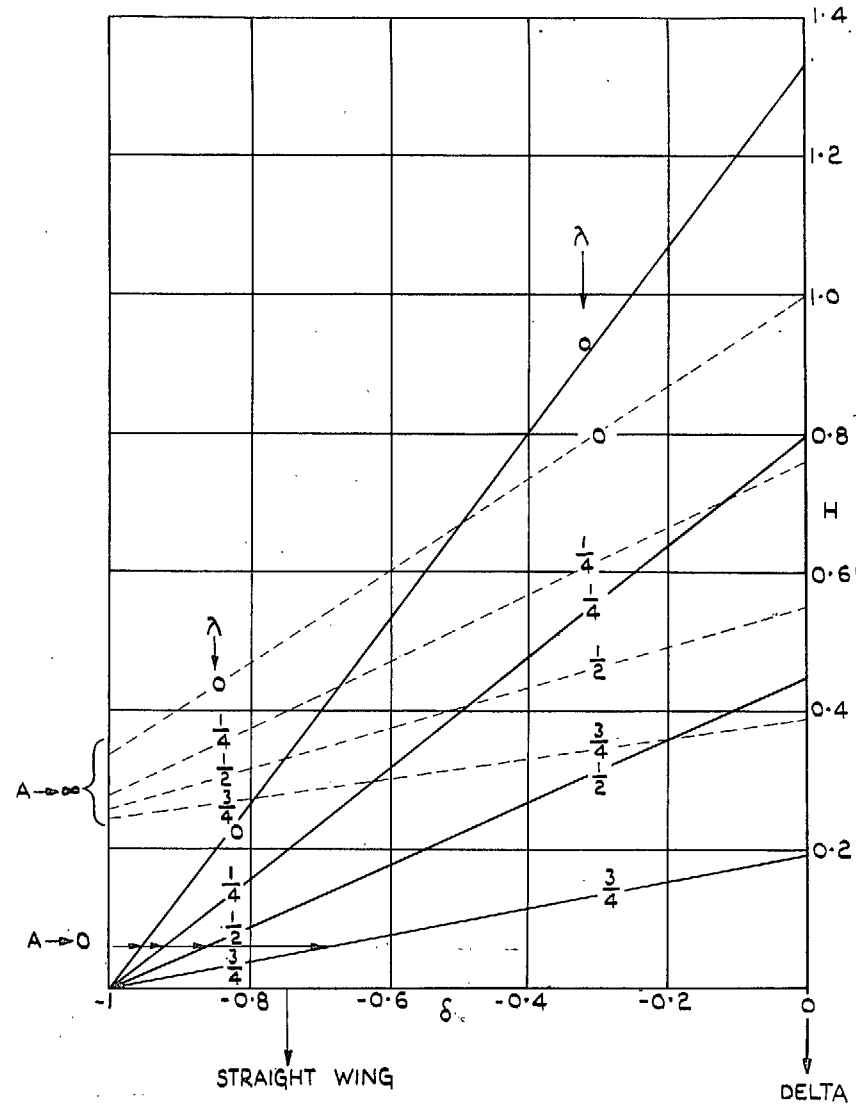

FIG. 12. Limiting positions of aerodynamic centre for large and small aspect ratio, δ negative.

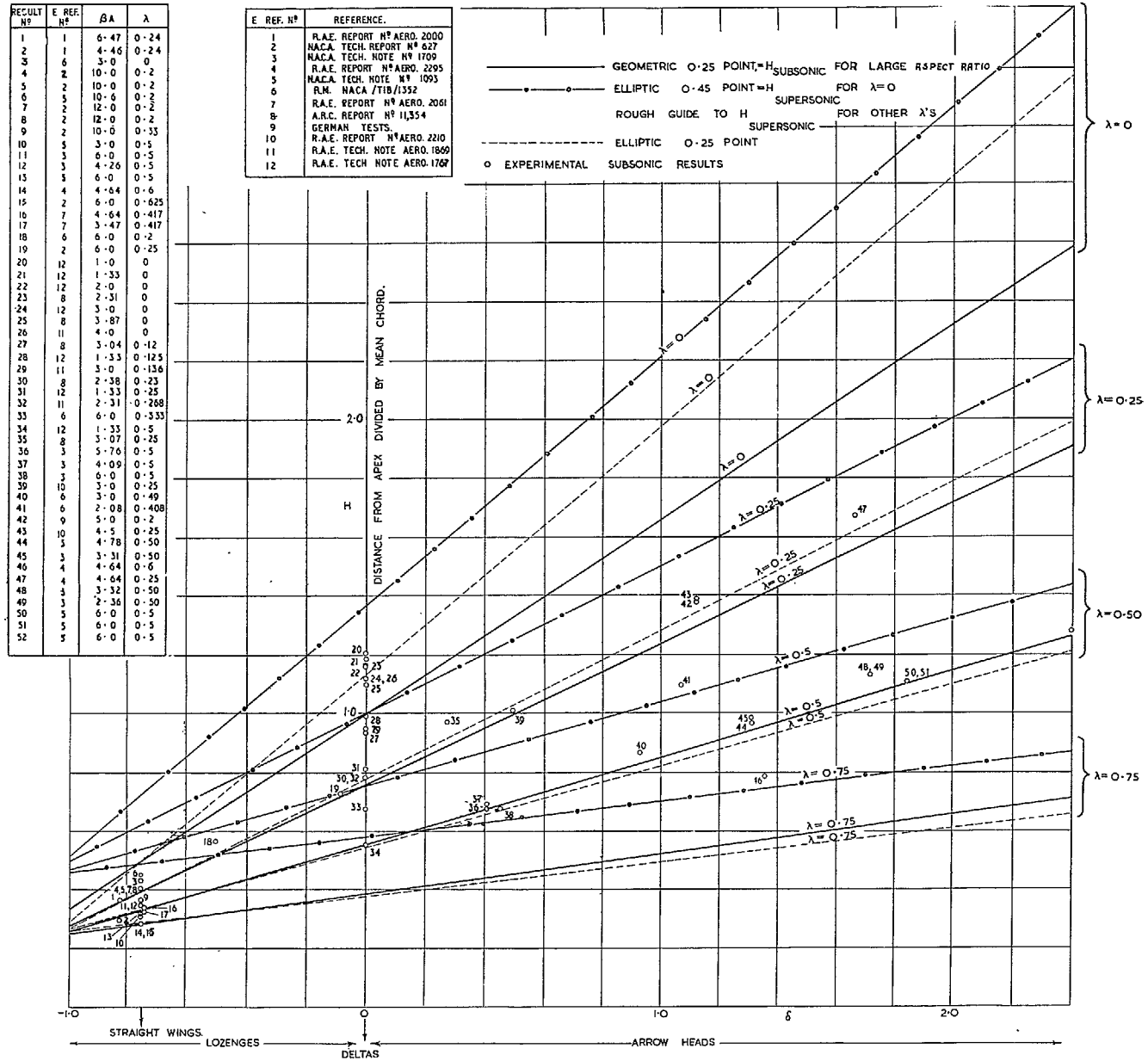

FIG. 13. Subsonic experimental results for aerodynamic centre of tapered wings.

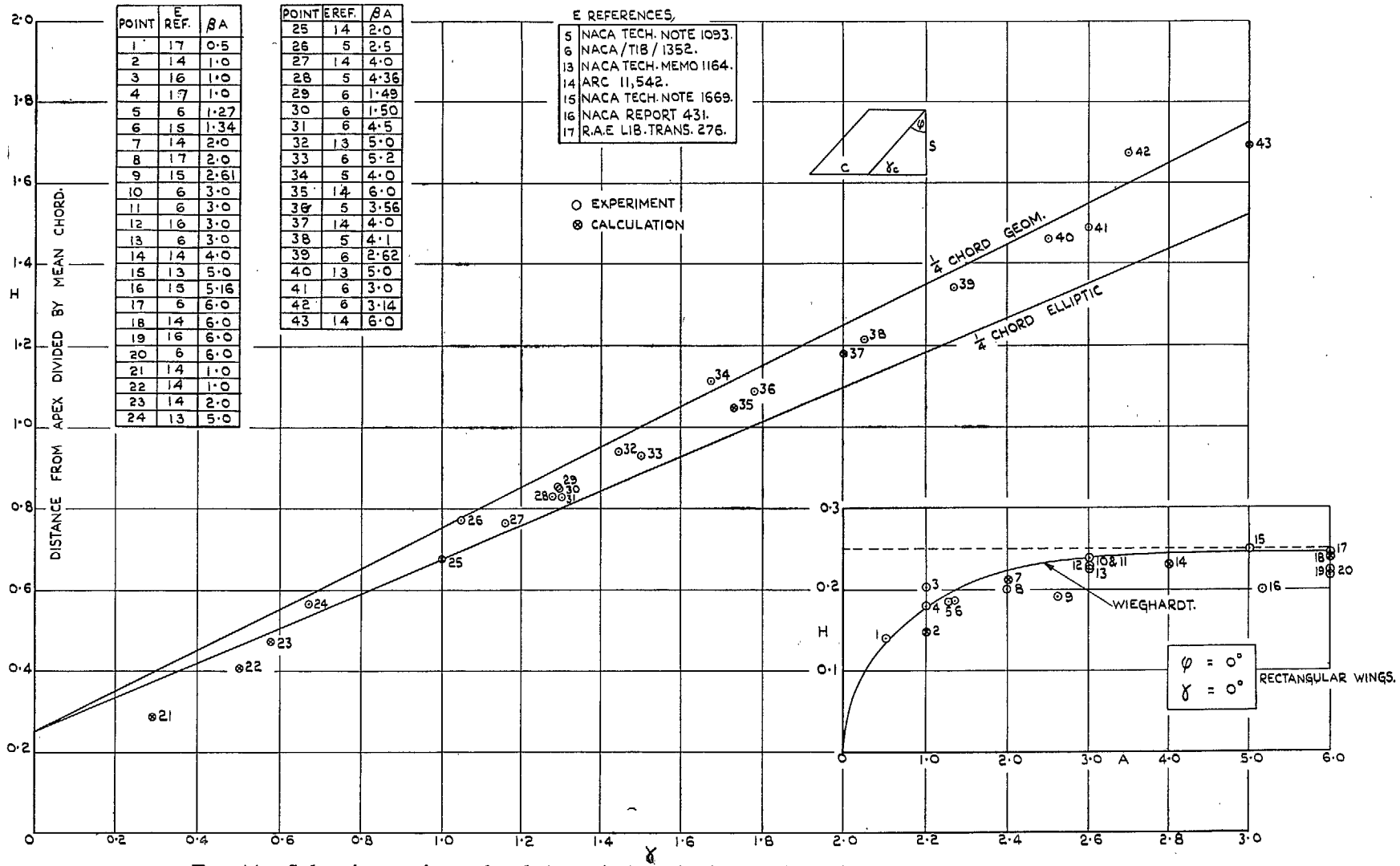

FIG. 14. Subsonic experimental and theoretical results for aerodynamic centre of untapered wings.

(372) Wt. 18/9296 K7 2/56 Hw.

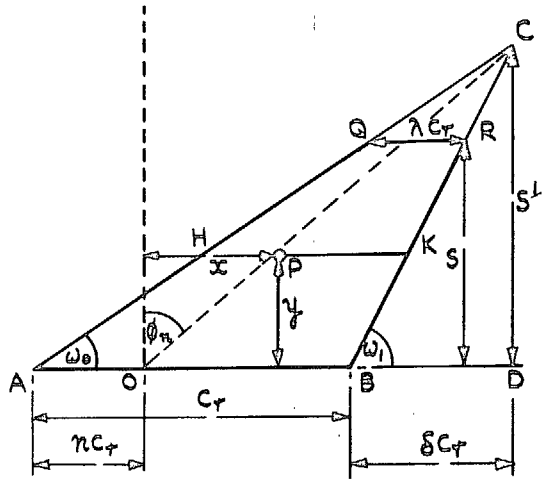

FIG. 15. Geometry to illustrate Appendix I.

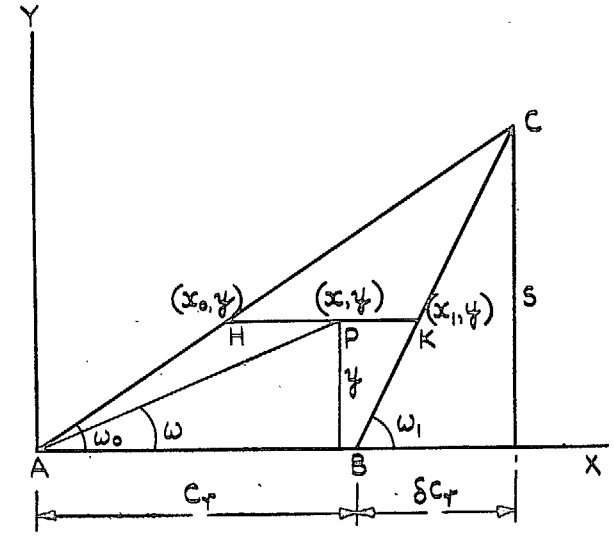

FIG. 16. Geometry to illustrate Appendix II.

PRINTED IN GREAT BRITAIN

Publications of the Aeronautical Research Council

ANNUAL TECHNICAL REPORTS OF THE AERONAUTICAL RESEARCH COUNCIL (BOUND VOLUMES)

1938 Vol. I. Aerodynamics General, Performance, Airscrews. 50*s.* (51*s.* 2*d.*)
Vol. II. Stability and Control, Flutter, Structures, Seaplanes, Wind Tunnels, Materials. 30*s.* (31*s.* 2*d.*)

1939 Vol. I. Aerodynamics General, Performance, Airscrews, Engines. 50*s.* (51*s.* 2*d.*)
Vol. II. Stability and Control, Flutter and Vibration, Instruments, Structures, Seaplanes, etc. 63*s.* (64*s.* 2*d.*)

1940 Aero and Hydrodynamics, Aerofoils, Airscrews, Engines, Flutter, Icing, Stability and Control, Structures, and a miscellaneous section. 50*s.* (51*s.* 2*d.*)

1941 Aero and Hydrodynamics, Aerofoils, Airscrews, Engines, Flutter, Stability and Control, Structures. 63*s.* (64*s.* 2*d.*)

1942 Vol. I. Aero and Hydrodynamics, Aerofoils, Airscrews, Engines. 75*s.* (76*s.* 3*d.*)
Vol. II. Noise, Parachutes, Stability and Control, Structures, Vibration, Wind Tunnels. 47*s.* 6*d.* (48*s.* 8*d.*)

1943 Vol. I. Aerodynamics, Aerofoils, Airscrews. 80*s.* (81*s.* 4*d.*)
Vol. II. Engines, Flutter, Materials, Parachutes, Performance, Stability and Control, Structures. 90*s.* (91*s.* 6*d.*)

1944 Vol. I. Aero and Hydrodynamics, Aerofoils, Aircraft, Airscrews, Controls. 84*s.* (85*s.* 8*d.*)
Vol. II. Flutter and Vibration, Materials, Miscellaneous, Navigation, Parachutes, Performance, Plates and Panels, Stability, Structures, Test Equipment, Wind Tunnels. 84*s.* (85*s.* 8*d.*)

Annual Reports of the Aeronautical Research Council—

1933–34	1*s.* 6*d.* (1*s.* 8*d.*)	1937	2*s.* (2*s.* 2*d.*)
1934–35	1*s.* 6*d.* (1*s.* 8*d.*)	1938	1*s.* 6*d.* (1*s.* 8*d.*)
April 1, 1935 to Dec. 31, 1936	4*s.* (4*s.* 4*d.*)	1939–48	3*s.* (3*s.* 2*d.*)

Index to all Reports and Memoranda published in the Annual Technical Reports, and separately—

April, 1950 — R. & M. No. 2600 — 2*s.* 6*d.* (2*s.* 7½*d.*)

Author Index to all Reports and Memoranda of the Aeronautical Research Council—

1909–January, 1954. — R. & M. No. 2570 — 15*s.* (15*s.* 4*d.*)

Indexes to the Technical Reports of the Aeronautical Research Council—

December 1, 1936 — June 30, 1939	R. & M. No. 1850	1*s.* 3*d.* (1*s.* 4½*d.*)
July 1, 1939 — June 30, 1945	R. & M. No. 1950	1*s.* (1*s.* 1½*d.*)
July 1, 1945 — June 30, 1946	R. & M. No. 2050	1*s.* (1*s.* 1½*d.*)
July 1, 1946 — December 31, 1946	R. & M. No. 2150	1*s.* 3*d.* (1*s.* 4½*d.*)
January 1, 1947 — June 30, 1947	R. & M. No. 2250	1*s.* 3*d.* (1*s.* 4½*d.*)

Published Reports and Memoranda of the Aeronautical Research Council—

Between Nos. 2251–2349	R. & M. No. 2350	1*s.* 9*d.* (1*s.* 10½*d.*)
Between Nos. 2351–2449	R. & M. No. 2450	2*s.* (2*s.* 1½*d.*)
Between Nos. 2451–2549	R. & M. No. 2550	2*s.* 6*d.* (2*s.* 7½*d.*)
Between Nos. 2551–2649	R. & M. No. 2650	2*s.* 6*d.* (2*s.* 7½*d.*)

Prices in brackets include postage

HER MAJESTY'S STATIONERY OFFICE

York House, Kingsway, London W.C.2 ; 423 Oxford Street, London W.1 (Post Orders : P.O. Box 569, London S.E.1), 13a Castle Street, Edinburgh 2 ; 39 King Street, Manchester 2 ; 2 Edmund Street, Birmingham 3 ; 109 St. Mary Street, Cardiff ; Tower Lane, Bristol, 1 ; 80 Chichester Street, Belfast, *or through any bookseller*

S.O. Code No. 23-2785